bioRxiv preprint doi: https://doi.org/10.1101/789057; this version posted October 1, 2019. The copyright holder for this preprint (which was not certified by peer review) is the author/funder, who has granted bioRxiv a license to display the preprint in perpetuity. It is made available under aCC-BY-NC-ND 4.0 International license.

Optogenetic modulation of TDP-43 oligomerization fast-forwards ALS-related pathologies in the spinal motor neurons

Kazuhide Asakawa[1, 2, 3, *], Hiroshi Handa[1], Koichi Kawakami[2, 3, *]

[1] Department of Nanoparticle Translational Research, Tokyo Medical University, Shinjuku, 160-8402, Japan

[2] Division of Molecular and Developmental Biology, National Institute of Genetics, 1111 Yata, Mishima, Shizuoka, Japan, 411-8540

[3] Department of Genetics, Graduate University for Advanced Studies (SOKENDAI), 1111 Yata, Mishima, Shizuoka, Japan, 411-8540

* Corresponding authors

Corresponding authors

Kazuhide Asakawa (Email: kasakawa@nig.ac.jp)

Koichi Kawakami (Email: kokawaka@nig.ac.jp)

bioRxiv preprint doi: https://doi.org/10.1101/789057; this version posted October 1, 2019. The copyright holder for this preprint (which was not certified by peer review) is the author/funder, who has granted bioRxiv a license to display the preprint in perpetuity. It is made available under aCC-BY-NC-ND 4.0 International license.

Abstract

Cytoplasmic aggregation of TDP-43 characterizes degenerating neurons in most cases of amyotrophic lateral sclerosis (ALS), yet the mechanisms and cellular outcomes of TDP-43 pathology remain largely elusive. Here, we develop an optogenetic TDP-43 variant (opTDP-43), whose multimerization status can be modulated *in vivo* through external light illumination. Using the translucent zebrafish neuromuscular system, we demonstrate that short-term light stimulation reversibly induces cytoplasmic opTDP-43 mislocalization, but not aggregation, in the spinal motor neuron, leading to an axon outgrowth defect associated with myofiber denervation. In contrast, opTDP-43 forms pathological aggregates in the cytoplasm after longer-term illumination and seeds non-optogenetic TDP-43 aggregation. Furthermore, we find that an ALS-linked mutation in the intrinsically disordered region (IDR) exacerbates the light-dependent opTDP-43 toxicity on locomotor behavior. Together, our results propose that IDR-mediated TDP-43 oligomerization triggers both acute and long-term pathologies of motor neurons, which may be relevant to the pathogenesis and progression of ALS.

bioRxiv preprint doi: https://doi.org/10.1101/789057; this version posted October 1, 2019. The copyright holder for this preprint (which was not certified by peer review) is the author/funder, who has granted bioRxiv a license to display the preprint in perpetuity. It is made available under aCC-BY-NC-ND 4.0 International license.

Introduction

Amyotrophic lateral sclerosis (ALS) is a neurological disorder in which the upper and lower motor neurons progressively degenerate, leading to muscular atrophy and eventually fatal paralysis. Trans-activation response element (TAR) DNA-binding protein 43 (TDP-43), a heterogeneous nuclear ribonucleoprotein, is mislocalized to the cytoplasm and forms pathological aggregates in the degenerating motor neurons in ALS [1, 2]. TDP-43 aggregation characterizes almost all cases of sporadic ALS [3, 4], which accounts for greater than 90% of ALS. Moreover, mutations in the *TARDBP* gene encoding TDP-43 are linked to certain fraction (~ 4 %) of familial ALS [5]. Despite its correlation with and causation of ALS, the role of TDP-43 in ALS pathogenesis has been largely unknown at the mechanistic level.

Multimerization of TDP-43 underlies its physiological and pathological roles. Under normal physiological conditions, homo-oligomerization of TDP-43 occurs through its N-terminal domain and is necessary for its RNA regulatory functions, such as splicing [6-8]. At the C-terminus TDP-43 contains an intrinsically disordered region (IDR) with prion-like glutamine/asparagine-rich (Q/N) and glycine-rich regions, which can undergo liquid-liquid phase separation (LLPS) to form dynamic protein droplets [9]. The TDP-43 IDR mutations that are linked to familial ALS cases enhance intrinsic aggregation propensity and protein stability of TDP-43 [10] [11] and result in altered phase separation [9], which could contribute to disease propagation through acceleration of the formation and accumulation of pathological aggregates [12, 13] [14]. The modular architecture of TDP-43 has led to several hypotheses that its N-terminus-dependent oligomerization modulates C-terminal IDR-mediated aggregation either by enhancing [9] or hindering IDR interactions between adjacent TDP-43 molecules [6] [15].

The severity of TDP-43 toxicity is correlated with the levels of wild-type and mutant TDP-43 expression in the various cellular and animal models [16-25]. However, cytoplasmic TDP-43 aggregation is not always detectable in these models. Moreover, in a certain type of degenerating upper motor neurons, loss of nuclear TDP-43 can occur

bioRxiv preprint doi: https://doi.org/10.1101/789057; this version posted October 1, 2019. The copyright holder for this preprint (which was not certified by peer review) is the author/funder, who has granted bioRxiv a license to display the preprint in perpetuity. It is made available under aCC-BY-NC-ND 4.0 International license.

without the accumulation of cytoplasmic aggregates [26]. Therefore, it has been difficult to evaluate how TDP-43 aggregation contributes to TDP-43 toxicity. Under these circumstances, it is necessary to develop a system to induce TDP-43 aggregation conditionally. Recently, light-dependent aggregation of *Arabidopsis* cryptochrome-2 was applied to the formation of IDR droplets via LLPS in a light illumination-dependent manner [27]. This optogenetic approach has been successfully extended to the induction of cytotoxic TDP-43 aggregates formation in cultured cells [28, 29]. However, interconversion of normal and toxic TDP-43 forms with spatiotemporal precision has not been achieved in animal models yet, which is central for the understanding of TDP-43 toxicity *in vivo*.

In the present study, we develop an optogenetic TDP-43 variant (opTDP-43) carrying a light-dependent oligomerization module of cryptochrome-2 attached to the IDR, and analyze the mechanisms of TDP-43 toxicity in spinal motor neurons *in vivo*. Transgenic expression and light stimulation of opTDP-43 in transparent zebrafish larvae show that oligomerization and aggregation of opTDP-43 is inducible and tunable by external light illumination *in vivo*. We reveal that, in the spinal motor neurons, short-term light illumination reversibly increases the cytoplasmic opTDP-43 pool and elevates myofiber denervation frequency in the absence of distinct aggregate formation. Furthermore, longer chronic light stimulation eventually leads to accumulation of cytoplasmic opTDP-43 aggregates that further seed aggregation of non-optogenetic TDP-43, which is accompanied by motor decline. The sequential pathological alterations of spinal motor neurons triggered by opTDP-43 oligomerization may provide clues about how motor neuron degeneration progresses at both molecular and cellular levels in a prodromal phase of ALS.

bioRxiv preprint doi: https://doi.org/10.1101/789057; this version posted October 1, 2019. The copyright holder for this preprint (which was not certified by peer review) is the author/funder, who has granted bioRxiv a license to display the preprint in perpetuity. It is made available under aCC-BY-NC-ND 4.0 International license.

Results

Overexpression of TDP-43 causes cytoplasmic aggregation-independent toxicity in the spinal motor neurons

To explore mechanisms of TDP-43 toxicity associated with its cytoplasmic aggregation in spinal motor neurons, we first aimed to induce TDP-43 aggregation by its overexpression in the caudal primary motor neurons (CaPs) of zebrafish, which innervate a ventral third of the myotome and are present uniquely in every spinal hemisegment (Figure1A, B) [30]. We generated a Gal4-inducible transgene of the zerbafish *tardbp*, encoding one of the two zebrafish TDP-43 paralogues, tagged with mRFP1 at its N-terminus (mRFP1-TDP-43z) (Figure 1C). To test the functionality of mRFP1-TDP-43z as TDP-43, we generated knock-out (KO) alleles for both *tardbp* and its paralogue *tardbpl* with the CRISPR-Cas9 system (i.e. *tardbp-n115* and *tardbpl-n94*, respectively). The TDP-43 double knock-out (DKO) embryos exhibited a blood circulation defect at 24-48 hours post-fertilization (hpf) (Sup. Figure 1D) and were lethal [31]. We injected mRNA encoding wild-type Tardbp and mRFP1-TDP-43z into the TDP-43 DKO embryos at the one-cell stage (Sup. Figure 1A, B, C) and found that the mutant phenotype was rescued by both, indicating that mRFP1-TDP-43 is functional (Sup. Figure 1E). We then overexpressed mRFP1-TDP-43z in CaPs by combining Tg[UAS:mRFP1-TDP-43z] with the Tg[SAIG213A] driver (Figure 1A, B) [32], and analyzed their muscle innervation. The mRFP-TDP-43z overexpression significantly reduced the total axonal length at 48 hpf (Figure 1C, D, E, Sup Movie 1), while the axon arborized within the inherent innervation territory of the ventral myotomes (Figure 1C, D) and their branching frequency (i.e. branching as calculated per total axon length) were comparable to that of the wild-type CaP (Figure 1F), showing that overexpression of mRFP-TDP-43z primarily affects axon outgrowth, but not pathfinding or branching. However, the overexpressed mRFP-TDP-43z was predominantly accumulated in the nucleus and cytoplasmic aggregation was undetectable in the CaP at 48 hpf (Figure 1G).

bioRxiv preprint doi: https://doi.org/10.1101/789057; this version posted October 1, 2019. The copyright holder for this preprint (which was not certified by peer review) is the author/funder, who has granted bioRxiv a license to display the preprint in perpetuity. It is made available under aCC-BY-NC-ND 4.0 International license.

These observations suggest that an elevated level of TDP-43 causes neurotoxicity independently of cytoplasmic aggregation in the spinal motor neurons.

A photo-switchable TDP-43: opTDP-43

Next, we developed an alternative strategy to induce cytoplasmic TDP-43 aggregation. The IDR at the C-terminal of TDP-43 has a high propensity to form aggregates [10]. Therefore, we reasoned that cytoplasmic TDP-43 aggregation might effectively occur when the proximity between IDRs was increased by addition of an exogenous multimerization tag, such as *Arabidopsis* cryptochrome CRY2. We first tested the feasibility of CRY2 oligomerization in spinal motor neurons *in vivo* via external light illumination. We created a transgenic zebrafish line carrying a fusion of mRFP1 and CRY2olig, a point mutant version of CRY2 (E490G) that exhibits significant clustering upon blue light illumination [33], under the UAS sequence (Figure 2A; Tg[UAS:mRFP1-CRY2olig]). In Tg[SAIG213A] Tg[UAS:mRFP1-CRY2olig] double transgenic embryos raised under dark conditions, mRFP1-CRY2olig was dispersed throughout the CaPs at 30 hpf (Figure 2B). Upon blue light illumination via confocal laser scanning of entire CaPs, mRFP1-CRY2olig instantaneously clustered in somas and axons during the first 10 min of illumination (Figure 2B, Sup Movie 2). Once illumination ceased, the mRFP1-CRY2olig clusters gradually disappeared and a homogeneous distribution of mRFP1-CRY2olig was restored (Figure 2B), showing that CRY2olig clustering is rapidly and reversibly controllable by light in the spinal motor neurons *in vivo*.

To adopt the clustering capacity of mRFP1-CRY2olig to TDP-43, we inserted the zebrafish *tardbp* between the mRFP1 and CRY2olig modules, and designated the resulting mRFP1-*tardbp*-CRY2olig fusion gene as opTDP-43z (i.e. optogenetic TDP-43 of zebrafish) (Figure 2A). The resulting opTDP-43z rescued the blood circulation defect of TDP-43DKO embryos under dark conditions as efficiently as wild-type *tardbp* (Sup Figure 1E), confirming that opTDP-43z is functional. We first assessed the

bioRxiv preprint doi: https://doi.org/10.1101/789057; this version posted October 1, 2019. The copyright holder for this preprint (which was not certified by peer review) is the author/funder, who has granted bioRxiv a license to display the preprint in perpetuity. It is made available under aCC-BY-NC-ND 4.0 International license.

oligomerization capacity of optoTDP-43z in the skeletal muscle cells by taking advantage of their relatively large nucleus and cytoplasm. Since the strong whole body expression of mRFP-TDP-43z driven by the ubiquitous Gal4 driver Tg[SAGFF73A] perturbed development (Sup. Figure 2), we generated a UAS transgenic line that expressed a tolerable level of opTDP-43z with the Tg[SAGFF73A] driver (Figure 2A; Tg[UAS:opTDP-43z]). Unlike mRFP1-CRY2olig, opTDP-43z predominantly localized to the nucleus of the skeletal muscle cells under dark conditions (Figure 2C), suggesting that opTDP-43z localization is regulated by TDP-43-dependent mechanisms. We found that, while the nuclear-enriched opTDP-43z localization persisted during the 3.5 hours of blue light illumination (28-31.5 hpf), the cytoplasmic opTDP-43z gradually increased (Figure 2C, Sup Movie 3) and opTDP-43z droplets appeared 60-90 min after the initiation of illumination (Figure 2C, D). On the other hand, the nuclear opTDP-43z signal decreased slightly but significantly over time during the illumination (Figure 2E). We also found that the cytoplasmic opTDP-43z droplets were partially ubiquitinated as shown by immunofluorescence (Figure 2F), suggesting that the opTDP-43z level is regulated by proteolysis [34, 35]. Altogether, these observations demonstrate that opTDP-43z is a photo-switchable variant of TDP-43 that forms aggregates in a blue light illumination-dependent manner.

Light stimulation of opTDP-43z promotes cytoplasmic mislocalization in neuronal cells

To investigate light responsiveness of opTDP-43z in neuronal cells, we expressed opTDP-43z in both spinal motor neurons and tactile sensing Rohon-Beard (RB) cells by combining both Tg[mnr2b-hs:Gal4] [36] and Tg[SAIG213A] drivers. Under dark conditions, opTDP-43z primarily localized to the nucleus of both cell types at 28 hpf in Tg[mnr2b-hs:Gal4] Tg[SAIG213A] Tg[UAS:opTDP-43z] Tg[UAS:EGFP] quadruple transgenic fish (Figure 3A). Upon blue light illumination of the spinal cord, the nuclear-enriched localization of opTDP-43z persisted for about 90 min in both spinal

bioRxiv preprint doi: https://doi.org/10.1101/789057; this version posted October 1, 2019. The copyright holder for this preprint (which was not certified by peer review) is the author/funder, who has granted bioRxiv a license to display the preprint in perpetuity. It is made available under aCC-BY-NC-ND 4.0 International license.

motor neurons and RB cells, and then its localization was gradually expanded to the entire EGFP-positive area (Figure 3B C, Sup Movie 4), suggesting that light-dependent opTDP-43z oligomerization promotes its mislocalization to the cytoplasm. Unexpectedly, however, the cytoplasmic opTDP-43z mislocalization did not lead to distinct droplet formation as observed in the skeletal muscle cells within the time frames examined (up to 4.5 hours illumination), suggesting that the spinal motor neurons and RB cells have lower propensity to form opTDP-43 aggregates than the skeletal muscle cells. The cell type-dependent variation of opTDP-43 mislocalization and aggregation was also substantiated by the observations that neither embryonic epithelial cells nor differentiated skeletal muscle fibers displayed cytoplasmic mislocalization or aggregation of opTDP-43z under the same light illumination condition (Sup Figure 3).

opTDP-43z oligomerization perturbs axon outgrowth

To explore the impact of light-induced opTDP-43z mislocalization at the whole cell level, we restricted opTDP-43z expression to CaPs by using the Tg[SAIG213A] driver. We devised a protocol by which Tg[SAIG213A] Tg[UAS:EGFP] Tg[UAS:opTDP-43z] triple transgenic fish were raised under continuous dark conditions until 48 hpf except being illuminated for 3 hours during 28-31 hpf (Figure 4A). Under this paradigm, opTDP-43z was primarily localized within the nucleus at 28 hpf, then dispersed throughout the nucleus and cytoplasm upon illumination, and restored its nuclear-enriched localization at 48-50 hpf (Figure 4A, B). We found by morphological analyses that total axon length, but not branching frequency, of CaPs decreased at 48-50 hpf by 13 % in the fish treated with 3 hours of blue light illumination, while such a phenotype was detected neither under continuous dark conditions nor by mRFP1-CRY2olig expression (Figure 4C, D, E). As observed with mRFP1-TDP-43z overexpression (Figure 1), the axons of light-stimulated CaPs expressing opTDP-43z arborized within their inherent ventral innervation territory (Figure 4C), and their branching frequency remained unchanged (Figure 4E), suggesting that the

bioRxiv preprint doi: https://doi.org/10.1101/789057; this version posted October 1, 2019. The copyright holder for this preprint (which was not certified by peer review) is the author/funder, who has granted bioRxiv a license to display the preprint in perpetuity. It is made available under aCC-BY-NC-ND 4.0 International license.

light-dependent opTDP-43z toxicity primarily influences axon outgrowth, but not pathfinding or branching.

The absence of distinct cytoplasmic aggregate formation in the CaPs raises the possibility that opTDP-43z exerts its toxicity through dragging of non-optogenetic TDP-43 out of the nucleus to the cytoplasm. To test this possibility, we constructed Tg[mnr2b-hs:EGFP-TDP-43z] expressing EGFP-TDP-43z under the control of the mnr2b promoter, and established a Tg[SAIGFF213A] Tg[UAS:opTDP-43z] Tg[mnr2b-hs:EGFP-TDP-43z] triple transgenic fish. Under dark conditions at 28 hpf, both opTDP-43z and EGFP-TDP-43z exhibited nuclear localization with subnuclear distribution patterns similar to each other (Figure 4I). Contrary to our prediction, however, the nuclear-enriched EGFP-TDP-43z localization remained unaffected while opTDP-43z was dispersed throughout the soma with 4 hour-blue light illumination during 28-32 hpf (Figure 4I-K), demonstrating that light-induced opTDP-43z mislocalization occurs independently of the non-optogenetic TDP-43 pool. These observations suggest that the perturbation of axon outgrowth by light-stimulated opTDP-43z is unlikely to be caused by loss of TDP-43 function due to nuclear TDP-43 reduction or depletion.

Light-stimulated opTDP-43z elevates myofiber denervation frequency

The opTDP-43z-mediated axon outgrowth defects raised the question as to whether opTDP-43z perturbs axon extension or promotes axon shrinkage, or both. To address this, we analyzed a major axon collateral of CaP innervating the dorsal side of its innervation territory that had experienced tertial branching at 56 hpf (provisionally named *d*orsal axon *c*ollateral of *C*aP with *t*ertial branching: DCCT) (Figure 5A). Live imaging revealed that the total DCCT length increased by 26 % from 56 to 72 hpf, (Figure 5B, C) and formed one additional branch on average in Tg[SAIG213A] Tg[UAS:GFP] larvae. Intriguingly, we noticed that a minor but significant population of single CaPs (24 %) increased their total DCCT length with a decrease in the number

bioRxiv preprint doi: https://doi.org/10.1101/789057; this version posted October 1, 2019. The copyright holder for this preprint (which was not certified by peer review) is the author/funder, who has granted bioRxiv a license to display the preprint in perpetuity. It is made available under aCC-BY-NC-ND 4.0 International license.

of collateral branches (Figure 5D), indicating that normal DCCT outgrowth involves both extension and shrinkage, as the extension occurs more frequently. The expression of opTDP-43z itself did not affect the average DCCT outgrowth rate and branch number under dark conditions at 56 hpf (Figure 5D, E). On the other hand, the average DCCT growth rate significantly declined by 11 % with at 72 hpf, when CaPs expressing opTDP-43z had been illuminated for 3 hours (from 56 to 59 hpf) (Figure 5D). Remarkably, 28 % (5 out of 18 DCCTs) of the illuminated CaPs exhibited total DCCT lengths (Figure 5C), and 44 % showed reduced DCCT branch number (Figure 5E), demonstrating that axon shrinkage contributes to the observed axon outgrowth defects.

We then investigated whether the DCCT shrinkage involves myofiber denervation by live monitoring of pre- and postsynaptic structures with Vamp2-Venus and tdTomato-tagged acetylcoline receptor (dT-chrnd), respectively (Figure 5F) [36]. We found that, in both wild-type and opTDP-43z expression conditions prior to light stimulation, the DCCT axon terminals were decorated by Vamp2-Venus and the Vamp2-Venus signals were well colocalized with dT-chrnd (Figure 5F, G), indicating normal neuromuscular assembly (Figure 5F). Live imaging revealed that, in the opTDP-43z-expressing CaPs after the 3 hours of illumination (during 56-59 hpf), Vamp2-Venus and juxtaposed dT-chrnd speckles at the axon terminal disappeared (Figure 5I), demonstrating that a decrement in DCCT terminal number is accompanied by myofiber denervation (Figure 5E). Such disappearance of juxtaposed Vamp2-Venus and dT-chrnd was also observed in wild-type DCCTs (Figure 5E, H). Overall, these observations show that the DCCT shrinkage is associated with myofiber denervation, and that optogenetic TDP-43 oligomerization raises the denervation frequency.

Cytoplasmic aggregation of opTDP-43h that seeds non-optogenetic TDP-43 aggregation in the spinal motor neurons

Targeted optogenetic stimulation via confocal laser scanning required the fish to be agarose-embedded, which restricted the illumination duration to a maximum of ~4

bioRxiv preprint doi: https://doi.org/10.1101/789057; this version posted October 1, 2019. The copyright holder for this preprint (which was not certified by peer review) is the author/funder, who has granted bioRxiv a license to display the preprint in perpetuity. It is made available under aCC-BY-NC-ND 4.0 International license.

hours fully maintain fish viability. We aimed to test if a longer illumination period potentially induces cytoplasmic aggregation of the optogenetic TDP-43 in the spinal motor neurons. We constructed transgenic fish in which most of the spinal motor neurons expressed a CRY2olig-tagged human TDP-43 (opTDP-43h, for optogenetic TDP-43 of human) from an mnr2b-BAC transgene (Tg[mnr2b-hs:opTDP-43h]) (Figure 6A)(Sup. Figure 1E)[31] and established a system for longitudinal field illumination of blue LED light using unrestrained fish. The Tg[mnr2b-hs:opTDP-43h] and Tg[mnr2b-hs:EGFP-TDP-43z] transgenes were combined to allow for simultaneous live monitoring of opTDP-43h and non-optogenetic TDP-43 in the spinal motor neurons. Prior to the illumination, both opTDP-43h and EGFP-TDP-43z were primarily localized in the nucleus at 2 days post-fertilization (dpf) (Figure 6B). We found that opTDP-43h was dispersed throughout the cell and formed aggregates in the cytoplasm at 3 dpf, and that aggregation was further enhanced over the subsequent 48 hours of illumination (i.e. 3-5 dpf). Despite distinct cytoplasmic opTDP-43h mislocalization and aggregation, EGFP-TDP-43z was predominantly localized to the nucleus during 2-4 dpf, suggesting that opTDP-43h mislocalization and aggregation occurred independently of EGFP-TDP-43z during the 48 hours of illumination. Intriguingly, at later time points (e.g. 5 dpf) when the cytoplasmic opTDP-43h developed into larger aggregates, EGFP-TDP-43z became detectable in the cytoplasm and formed distinct foci that colocalized with opTDP-43h aggregates (Figure 6C), indicating that, the long term light-induced opTDP-43h aggregates seeds aggregation of non-optogenetic TDP-43.

IDR mutation A315T enhances protein stability and oligomerization-dependent toxicity of TDP-43

The gradual mislocalization and aggregation of non-optogenetic TDP-43 promoted by the light-stimulated opTDP-43h prompted us to hypothesize that opTDP-43h first oligomerizes via the CRY2olig module and subsequently seeds non-optogenetic TDP-43 aggregation, via its aggregate-prone IDR [10, 37]. To test whether the IDR

bioRxiv preprint doi: https://doi.org/10.1101/789057; this version posted October 1, 2019. The copyright holder for this preprint (which was not certified by peer review) is the author/funder, who has granted bioRxiv a license to display the preprint in perpetuity. It is made available under aCC-BY-NC-ND 4.0 International license.

contributes to light-dependent toxicity of opTDP-43h, we created an opTDP-43 mutant with an IDR mutation (A315T) linked to familial ALS (opTDP-43h^{A315T}) and expressed opTDP-43h^{A315T} widely in the spinal motor neurons from Tg[mnr2b-hs:opTDP-43h^{A315T}]. In Tg[mnr2b-hs:opTDP-43h^{A315T}] Tg[mnr2b-hs:EGFP-TDP-43z] double transgenic fish, opTDP-43h^{A315T} displayed nuclear-enriched localization prior to the LED illumination at 48 hpf. We noted that the expression level of opTDP-43h^{A315T} protein was less than that of opTDP-43h in the Tg[mnr2b-hs:opTDP-43h] fish, partly due to the lower level of mRNA (Figure 6E). Nonetheless, in response to illumination, opTDP-43h^{A315T} mislocalized to the cytoplasm, formed aggregates within 24 hours of illumination and seeded cytoplasmic aggregates containing non-optogenetic EGFP-TDP-43z (Figure 6C, D). We then quantified the amounts of opTDP-43h and opTDP-43h^{A315T} proteins in the single cells before and after the initial 24 hours of illumination (2-3 dpf), by using EGFP-TDP-43z expressed from Tg[mnr2b-hs:EGFP-TDP-43z] as an internal control. the relative intensity of opTDP-43h^{A315T} significantly increased during the illumination by 3 dpf while that of opTDP-43h remained unchanged (Figure 6F, G, H), indicating that the A315T mutation increases the protein stability. This observation is consistent with the previous observations in cultured neurons [11, 38]. The illuminated Tg[mnr2b-hs:opTDP-43h] Tg[mnr2b-hs:EGFP-TDP-43z] larvae were viable with seemingly normal free-swimming activity at 5-6 dpf, suggesting that the toxicity associated with light-stimulated opTDP-43h has only a minor effect at the behavioral level. On the other hand, 18 % of the illuminated fish expressing opTDP-43h^{A315T}, but none of the non-illuminated siblings, failed to inflate the swim bladder at 5 dpf and showed declined locomotor ability (Figure 6I, Sup Movie 5), indicating that the A315T mutation enhances oligomerization-dependent toxicity of opTDP-43h. Altogether, these observations suggest that the IDR of TDP-43 causes the oligomerization-dependent toxicity in the spinal motor neurons.

Discussion

bioRxiv preprint doi: https://doi.org/10.1101/789057; this version posted October 1, 2019. The copyright holder for this preprint (which was not certified by peer review) is the author/funder, who has granted bioRxiv a license to display the preprint in perpetuity. It is made available under aCC-BY-NC-ND 4.0 International license.

Pathological aggregation of TDP-43 via the IDRs is proposed to be antagonized by N-terminal-mediated homo-oligomerization under physiological conditions [6, 15]. In this study, we successfully developed CRY2olig-mediated TDP-43 oligomerization system *in vivo* and demonstrated CRY2olig-mediated oligomerization led to the accumulation of cytoplasmic opTDP-43 aggregates in the zebrafish spinal motor neurons. This CRY2olig-driven opTDP-43 oligomerization would initially generate reversible interactions within the IDRs, some of which occasionally transform into an irreversible form. Then, such irreversible "knots" of opTDP-43 eventually seed IDR-mediated aggregation of non-optogenetic TDP-43 (Figure 7). Under our illumination conditions, the spinal motor neurons require up to 3 hours to fully disperse opTDP-43 throughout the cell, 24 hours to accumulate distinct cytoplasmic opTDP-43 aggregates, and several additional days to develop cytoplasmic opTDP-43 aggregates containing non-optogenetic TDP-43. This sequentially regulated illumination-triggered TDP-43 knot and aggregate formation enables direct observation of spinal motor neuron pathology as triggered by IDR-mediated TDP-43 oligomerization. We propose that this opTDP-43-triggered pathology may correspond to a fast-forwarding of spinal motor neuron degeneration in ALS, in which a majority of cases are believed to involve IDR-mediated TDP-43 aggregation, yet currently allows very restricted anatomical access.

We discovered that the reversible cytoplasmic opTDP-43 mislocalization induced by short-term light illumination was sufficient to cause defective motor axon outgrowth accompanied by enhanced myofiber denervation. The physiological nuclear-enriched TDP-43 localization is sustained by nucleocytoplasmic transport system [34, 35] as well as protein degradation systems in the cytoplasm, such as the ubiquitin proteasome system (UPS) and autophagy [39, 40]. Since the light-dependent cytoplasmic opTDP-43 mislocalization commences without affecting non-optogenetic TDP-43 localization, the toxicity accompanied by opTDP-43 mislocalization may not be caused by a global shutdown of nucleocytoplasmic transport or proteolysis systems

bioRxiv preprint doi: https://doi.org/10.1101/789057; this version posted October 1, 2019. The copyright holder for this preprint (which was not certified by peer review) is the author/funder, who has granted bioRxiv a license to display the preprint in perpetuity. It is made available under aCC-BY-NC-ND 4.0 International license.

for TDP-43, but rather by dysregulation of RNAs and/or proteins being bound by opTDP-43. TDP-43 can associate with more than 6,000 RNA targets [41-44], and RNA-binding is antagonistic to toxic TDP-43 oligomerization in an optogenetic cellular model [28], implying that light-dependent opTDP-43 oligomerization would profoundly affect its RNA-binding capacity, thereby influencing the expression of a myriad of genes. In terms of the axon outgrowth defect, whether toxicity is ascribable to dysregulation of specific key proteins [39, 45] or to a widespread translational abnormality [46], which could lead to stress-inducing misfolded protein accumulation, remains to be investigated. Nevertheless, the normal motor axon pathfinding and unaffected branching frequency suggest a certain specificity of opTDP-43 toxicity and would favor the idea that the cellular growth pathway is primarily affected by the toxicity. It should also be noted that our current illumination paradigm encompasses not only the somas but also the motor axons. Therefore, "resident" cytoplasmic opTDP-43, such as that included in mRNP granules undergoing axonal transport [47] and in mitochondria at the axon terminals [48, 49], could also be photoconverted *in situ*, thereby contributing to the acute toxicity that involves neuromuscular synapse destabilization. Spatially-resolved light stimulation, a major advantage of optogenetics, could identify such potentially multiple pathogenic origins in the future.

The light-dependent cytoplasmic opTDP-43 mislocalization provides unexpected insight into the relationships between TDP-43 multimerization, localization, and toxicity, given that a toxic level of mRFP1-TDP-43 overexpression led neither to cytoplasmic mislocalization nor aggregation. The persistent nuclear localization of overexpressed mRFP1-TDP-43 indicates a robustness of the nucleocytoplasmic transport and cytoplasmic protein degradation systems against proteostatic perturbation of TDP-43. On the other hand, these TDP-43 surveillance systems appear to be inert against the IDR-mediated TDP-43 oligomers, as evidenced by the light-dependent cytoplasmic opTDP-43 mislocalization. These manipulations of proteostasis and multimerization revealed that a dosage increase of TDP-43 does not immediately lead to

bioRxiv preprint doi: https://doi.org/10.1101/789057; this version posted October 1, 2019. The copyright holder for this preprint (which was not certified by peer review) is the author/funder, who has granted bioRxiv a license to display the preprint in perpetuity. It is made available under aCC-BY-NC-ND 4.0 International license.

IDR-mediated oligomerization in the spinal motor neurons, and therefore TDP-43 toxicity associated with proteostatic abrogation could be mechanistically distinct from that caused by IDR-mediated oligomerization. Importantly, our animal model approach explicitly revealed a striking cell-type variation of opTDP-43 mislocalization and aggregation, such that the neuronal cells are less prone to accumulate opTDP-43 aggregates compared to the differentiating muscle cells, while both of these cell types are inherently more competent for cytoplasmic mislocalization than the epithelial cells. Although the mechanisms underlying this cell-type specificity remain unknown, the present and previous observations [50] emphasize the importance of studying vulnerable cell types *in vivo* for accurately disclosing the mechanisms underlying TDP-43 localization, and thereby toxicity.

The verification that CRY2olig-mediated opTDP-43 oligomerization is toxic to the spinal motor neurons instead made it difficult to evaluate the toxicity derived from opTDP-43 aggregates alone, as the oligomeric and aggregate forms of opTDP-43 coexists during illumination. In this regard, it is noteworthy that the opTDP-43h^{A315T} that was expressed less and formed fewer cytoplasmic aggregates was more toxic than the opTDP-43h expressed in larger amounts (Figure 6), which provides an *in vivo* example in which the amount of accumulated TDP-43 aggregates does not necessarily predict the degree of TDP-43 toxicity [16, 17]. It was recently proposed that TDP-43 adopts both reversible and irreversible β-sheet aggregates that are involved in the formation of membraneless organelles, such as stress granules (SGs) and pathogenic amyloids, respectively, and that ALS mutations, including A315T, can promote the transition of such reversible to irreversible pathogenic aggregation [13]. Also, in frontotemporal lobar degeneration (FTLD), TDP-43 displays distinct aggregate assemblies and toxic effects in disease-subtype-specific manners [51]. Thus, it is possible that light-induced opTDP-43 aggregates are in fact heterogeneous and only a certain form of aggregates become pathogenic and acquire seeding activity for non-optogenetic TDP-43 aggregation. The time lag (~48 hours) between opTDP-43's own aggregation and subsequent

bioRxiv preprint doi: https://doi.org/10.1101/789057; this version posted October 1, 2019. The copyright holder for this preprint (which was not certified by peer review) is the author/funder, who has granted bioRxiv a license to display the preprint in perpetuity. It is made available under aCC-BY-NC-ND 4.0 International license.

393 opTDP-43-dependent non-optogenetic TDP-43 aggregation might represent the time
394 required for speciation of IDR interactions to develop such seeding capacity. The
395 toxicity of opTDP-43 aggregates should be evaluated by considering such potential
396 heterogeneity, and therefore remains as a challenging but important question to be
397 addressed. Alternatively, the seeding capacity for non-optogenetic TDP-43 aggregation
398 suggests that the toxicity of opTDP-43 aggregates can be exerted as a long-term effect
399 through gradual depletion of the available nuclear and cytoplasmic TDP-43 pools into
400 these aggregates, which would manifest as a TDP-43 loss-of-function phenotype.
401 It has been estimated that, even during healthy aging, the spinal motor
402 neurons are substantially lost [52-54]. As a result, the surviving motor units are enlarged to
403 preserve maximal force generating capacity by compensatory collateral reinnervation [55].
404 ALS has also been characterized by an elevated number of muscle fibers innervated by
405 a single subterminal axon [56], which is likely a remnant of such compensatory collateral
406 reinnervation events. In the present study, we found by live imaging of axon collateral
407 that an innervation territory of healthy spinal motor neurons is determined by a balance
408 between assembly and disassembly of neuromuscular synapses in zebrafish. We further
409 discovered that optogenetic opTDP-43 oligomerization could tip the balance toward
410 disassembly and decrease the total collateral length. Therefore, our results predict that,
411 once a cellular concentration of IDR-mediated TDP-43 oligomers reaches a critical
412 level, a spinal motor neuron would begin to reduce its motor unit size through repetition
413 of incomplete denervation/reinnervation cycles. Such neurons would also be defective
414 in complementing damaged neighboring motor units through collateral reinnervation,
415 which would accelerate the manifestation of motor decline. We envision that opTDP-43
416 allows for approaching the mechanisms underlying such dynamic
417 innervation/reinnervation balancing of spinal motor axons in health and
418 TDP-43-associated pathology, as well as for interrogating how not only motor neurons
419 but also diverse types of surrounding cells, including muscle, glial and endothelial cells,
420 respond to and modify TDP-43 toxicity. Moreover, combined with the feasibility of

bioRxiv preprint doi: https://doi.org/10.1101/789057; this version posted October 1, 2019. The copyright holder for this preprint (which was not certified by peer review) is the author/funder, who has granted bioRxiv a license to display the preprint in perpetuity. It is made available under aCC-BY-NC-ND 4.0 International license.

high-throughput, whole organism chemical screening in zebrafish, opTDP-43-mediated motor neuron pathogenesis should be extended for exploring small molecules that restore a normal denervation/reinnervation balance for spinal motor neurons, which might serve as drugs for ALS and other TDP-43 proteinopathy.

Acknowledgements

Authors would like to thank Drs Keiko Imamura and Haruhisa Inoue for valuable discussions and Kawakami lab members for generous support. This work was supported by SERIKA FUND (KA), The Nakabayashi Trust For ALS Research (KA), THE KATO MEMORIAL TRUST FOR NAMBYO RESEARCH (KA), Daiichi-Sankyo Foundation of Life Science (KA), Takeda Science Foundation (KA), KAKENHI Grant numbers JP16K07045 (KA), JP19K06933 (KA), National BioResource Project from Japan Agency for Medical Research and Development (AMED) (K.K.), and KAKENHI Grant Numbers JP15H02370 (K.K.).

Author contributions

KA conceived the research, designed and performed the experiments. KA and KK analyzed the data and wrote the manuscript with inputs from HH.

Competing Interests

KA and KK have filed a patent application (JP2018-186569) based on this work with the Japan Patent Office.

Methods

Fish lines

This study was carried out in accordance with the Guide for the Care and Use of Laboratory Animals of the Institutional Animal Care and Use Committee (IACUC, approval identification number 24-2) of the National Institute of Genetics (NIG, Japan),

bioRxiv preprint doi: https://doi.org/10.1101/789057; this version posted October 1, 2019. The copyright holder for this preprint (which was not certified by peer review) is the author/funder, who has granted bioRxiv a license to display the preprint in perpetuity. It is made available under aCC-BY-NC-ND 4.0 International license.

449 which has an Animal Welfare Assurance on file (assurance number A5561-01) at the
450 Office of Laboratory Animal Welfare of the National Institutes of Health (NIH, USA).
451 Fish were raised under 12:12 light-dark (L/D) cycles during the first 5 days after birth,
452 unless otherwise stated.
453
454 *Transgenic fish lines*
455 Tg[UAS:mRFP1-TDP-43z] was generated by synthesizing a *Tol2* transposon-based
456 cassette (UAS:mRFP1-TDP-43z) carrying the zebrafish *tardbp* (Genbank accession #
457 NM_2014476) that was tagged with mRFP1 (Genbank accession # AF506027.1) at the
458 N-terminus with linker peptide and placed downstream of x5 upstream activation
459 sequence (UAS)[57] (pBMH-T2ZUASRzT43, Biomatik). For constructing
460 Tg[UAS:mRFP1-CRY2olig], the zebrafish codon-optimized photolyase homology
461 region (PHR) of *Arabidopsis thaliana* CRY2 carrying the E490G mutation
462 (CRY2olig)[33] was synthesized (Biomtik) and N-terminally tagged with mRFP1 with a
463 linker peptide TRDISIE encoded by ACG CGT GAT ATC TCG ATC GAG
464 (mRFP1-CRY2olig). The mRFP1-CRY2olig fragment was fused to 5xUAS, cloned into
465 the Tol2-transposon cassette. For the construction of Tg[UAS:opTDP-43z], the
466 mRFP1-TDP-43z fragment was C-terminally fused to CRY2olig with the linker peptide
467 TRDISIE (opTDP-43z). The opTDP-43z fragment was fused to 5xUAS, cloned into the
468 Tol2-transposon cassette. NEBuilder HiFi DNA Assembly Master Mix was used for the
469 vector construction. For the generation of Tg[mnr2b-hs:EGFP-TDP-43z], EGFP was
470 directly fused to zebrafish *tardbp* gene (EGFP-TDP-43z) and the resulting
471 EGFP-TDP-43z was linked to the *hsp70l* promoter (650 bp) and introduced into
472 downstream of the *mnr2b* 5'UTR in the *mnr2b*-BAC DNA (CH211-172N16, BACPAC
473 Resources Center) via homologous recombination using a Km^r-resistance as essentially
474 described [58]. Tg[mnr2b-hs:opTDP-43h] and Tg[mnr2b-hs:opTDP-43h^{A315T}] lines were
475 generated by the same procedure except that opTDP-43h and opTDP-43h ^{A315T} were
476 used, respectively, instead of EGFP-TDP-43z. The opTDP-43h consists of the

bioRxiv preprint doi: https://doi.org/10.1101/789057; this version posted October 1, 2019. The copyright holder for this preprint (which was not certified by peer review) is the author/funder, who has granted bioRxiv a license to display the preprint in perpetuity. It is made available under aCC-BY-NC-ND 4.0 International license.

zebrafish-codon-optimized human TDP-43 that is fused directly to the zebrafish-codon-optimized mRFP1 at the N-terminus and indirectly to CRY2olig via the linker peptide TRDISIE. opTDP-43h^{A315T} is identical to opTDP-43h except A315T mutation (GCT > ACT). All transgenic lines were created via *Tol2*-mediated transgenesis.

TDP-43 knockout

For the generation of *tardbp* and *tardbpl* knockout fish, target sequences for Cas9-mediated cleavage were searched by CRISPRscan [59]. The target sequences CAAGACTTAAAAGACTACTTcgg and CAAGACTTAAAAGACTACTTcgg, where the protospacer adjacent motifs (PAMs) are indicated by lower cases, were chosen for the generation of *tardbp-n115* and *tardbpl-n94* alleles, respectively. hSpCas9 was *in vitro*-transcribed with mMESSAGE mMACHINE Kit (Thermo Fisher Scientific, AM1340) by using pCS2+hSpCas9 plasmid as a template (a gift from Masato Kinoshita, Addgene plasmid # 51815). Wild type embryos were injected with 25 pg of sgRNA and 300 pg of hSpCas9 mRNA at the one-cell stage.

Rescue experiment of *TDP-43 knockout fish via mRNA injection*

For the expression of human and zebrafish TDP-43 and its derivatives via mRNA injection, the open reading frames of zebrafish *tardbp* (TDP-43z), zebrafish-codon optimized human TDP-43 (TDP-43h), mRFP1-tagged zebrafish *tardbp* (mRFP1-TDP-43z) and opTDP-43z was cloned into pCS2+ vector *in vitro*-transcribed with mMESSAGE mMACHINE Kit. First, we injected varied amount of TDP-43z mRNA into the offspring obtained from incrosses of parental zebrafish carrying homozygous *tardbp-n115* and heterozygous *tardbpl-n94* mutation or heterozygous *tardbp-n115* and homozygous *tardbpl-n94* mutation at the one cell stage. After investigating the presence or absence of blood flow at 36-48 hpf, all fish were subjected individually to genotyping for *tardbp-n115* and *tardbpl-n94* alleles. The uninjected

bioRxiv preprint doi: https://doi.org/10.1101/789057; this version posted October 1, 2019. The copyright holder for this preprint (which was not certified by peer review) is the author/funder, who has granted bioRxiv a license to display the preprint in perpetuity. It is made available under aCC-BY-NC-ND 4.0 International license.

505 *tardbp-n115 tardbpl-n94* double homozygotes displayed a swollen heart that was
506 beating, but the blood cells were completely stacked on the yolk surface and cannot
507 reach the heart. An injection of 150 ng of TDP-43z mRNA was the most effect effective
508 in restoring blood flow (up to 40% of the double homozygotes) of the double
509 homozygotes with a minimum developmental abnormality due to overexpression.
510 Throughout the assay, we scored that the blood flow was "rescued" when any blood cell
511 flowing through the beating heart was observed. The function of TDP-43h and TDP-43
512 derivatives were tested by the microinjection of 150 ng mRNA each. The *tardbpl-n115*
513 allele was identified by performing Heteroduplex Mobility Assay (HMA) against PCR
514 product obtained with a primer pair: *tardbp-6F3* (5'-gcc aga taa taa gag gaa gat gga-3')
515 and *tardbpl-6R3* (5'-tga cag tac aaa gac aaa cac cac-3'). The *tardbpl-n94* allele was
516 similarity identified by using a primer pair: *tardbpl-4F2* (5'-caa tca ctg aat gaa tgc act
517 ttt-3') and *tardbpl-4R2* (5'-gtt tgc tta tac taa cct gca cca-3').
518
519 *Blue light illumination*
520 Short-term (< 4 hours) light stimulations of mRFP1-CRY2olig and opTDP-43z were
521 carried out by embedding fish in the 0.8-1 % low-melting agarose (NuSieve® GTG®
522 Agarose, Lonza) and conducting confocal scanning with the laser with 473 nm wave
523 length using an Olympus FV1200 microscope. The average optical power of the
524 confocal laser was approximately 44.66 μW/cm^2. For longer-term illumination, fish
525 were raised in 6-well dish with 8 ml E3 buffer, and the dish was placed on a blue LED
526 panel.
527
528 *Immunohistochemistry*
529 For the mono- and polyubiquitinated protein staining, Tg[SAGFF73A]
530 Tg[UAS:opTDP-43z] fish at 31.5 hpf that had illuminated with a blue light were taken
531 out from the agarose and immediately subjected to immunohistochemistry. For short,
532 fish were fixed for 2 hours with PBS (pH 7.4) containing 4.0 % paraformaldehyde. The

bioRxiv preprint doi: https://doi.org/10.1101/789057; this version posted October 1, 2019. The copyright holder for this preprint (which was not certified by peer review) is the author/funder, who has granted bioRxiv a license to display the preprint in perpetuity. It is made available under aCC-BY-NC-ND 4.0 International license.

mouse monoclonal antibody for mono- and polyubiquitinate conjugates (1/100, FK2, Enzo) and goat anti-mouse Alexa Fluor 488 (1:1,000, Molecular Probes) were used as primary and secondary antibodies, respectively. To detect opTDP-43z, the Anti-RFP rabbit polyclonal antibody (pAb, MBL) and goat anti-rabbit Alexa Fluor 633 (1:1,000, Molecular Probes) were used as primary and secondary antibodies, respectively.

Microscopic analysis

For confocal microscopy, a live embryo or larva was embedded in 0.8-1 % low-melting agarose (NuSieve® GTG® Agarose, Lonza) on a Glass Base dish (IWAKI, 3010-035) and subject to confocal microscopy using an Olympus FV1200 laser confocal microscope. Images of live embryos and larvae were acquired as serial sections along the z-axis and analyzed with Olympus Fluoview Ver2.1b Viewer, Image J and Adobe Photoshop CS6. The axon length and branching frequency were measured by Imaris Filament Tracer. A neurite with more than 5 μm of length was counted as branch. Morphological analyses of CaP were restricted to the spinal segment 14-17 before 50 hpf and to 13-17 during 56–72 hpf. For the quantitation of opTDP-43z in the skeletal muscle cells, averaged change of opTDP-43 intensity in the cytoplasm (D) and nucleus (E) during the illumination (N = 8 cells). *, p = 0.0097. For quantitation of opTDP-43h fluorescence intensity over EGFP-TDP-43z in the spinal motor neurons, a z-stack image of the spinal motor column was first created by Sum Slices function of ImageJ. Then, the soma area was defined by the contour of weak cytosolic fluorescence of EGFP-TDP-43z and the fluorescent intensities of opTDP-43h and EGFP-TDP-43z in the soma area were measured for individual cells using imageJ software. Statistical analyses were performed using GraphPad Prism Software.

RT-PCR

The total RNA was prepared from Tg[mnr2b-hs:EGFP-TDP43z], Tg[mnr2b-hs:EGFP-TDP43z] Tg[mnr2b-hs:opTDP-43h], and

bioRxiv preprint doi: https://doi.org/10.1101/789057; this version posted October 1, 2019. The copyright holder for this preprint (which was not certified by peer review) is the author/funder, who has granted bioRxiv a license to display the preprint in perpetuity. It is made available under aCC-BY-NC-ND 4.0 International license.

Tg[mnr2b-hs:EGFP-TDP43z] Tg[mnr2b-hs:opTDP-43h^{A315T}] larvae at 72 hpf (17 larvae each) by homogenizing in 1 ml of Trizol Reagent (Life Technologies) . Three μg of the total RNA is used for cDNA synthesis using oligo dT (SuperScriptn®III First-Strand, Invitrogen). opTDP-43h and opTDP-43h^{A315T} were detected by a primer pair against the zebrafish codon-optimized mRFP1: zmRFP1-123f (5'-TCA GAC AGC TAA ACT GAA GGT CAC-3') and zmRFP1-633r (5'-GAC GAT GGT ATA GTC TTC GTT GTG-3'). EGFP-TDP-43z was detected by a primer pair against EGFP: EGFP-f2s (5'-CAC ATG AAG CAG CAC GAC TTC T-3') and EGFP-r5s (5'-ACG TTG TGG CTG TTG TAG TTG T-3'). zfand5b expression was detected by a primer pair: zfand5b--133f (5'-ATA GTA CAC ACC GAA ACG GAC AC-3') and zfand5b-772r (5'-TTA TAT TCT CTG GAT TTT ATC GGC-3')

Data availability

The data that support the findings in this study are available within the article and its Supplemental Information files, and from the corresponding authors upon request.

References

1. Arai, T. *et al*. TDP-43 is a component of ubiquitin-positive tau-negative inclusions in frontotemporal lobar degeneration and amyotrophic lateral sclerosis. *Biochem Biophys Res Commun* **351**, 602-611 (2006).
2. Neumann, M. *et al*. Ubiquitinated TDP-43 in frontotemporal lobar degeneration and amyotrophic lateral sclerosis. *Science* **314**, 130-133 (2006).
3. Mackenzie, I.R. *et al*. Pathological TDP-43 distinguishes sporadic amyotrophic lateral sclerosis from amyotrophic lateral sclerosis with SOD1 mutations. *Ann Neurol* **61**, 427-434 (2007).
4. Tan, C.F. *et al*. TDP-43 immunoreactivity in neuronal inclusions in familial amyotrophic lateral sclerosis with or without SOD1 gene mutation. *Acta Neuropathol* **113**, 535-542 (2007).
5. Lagier-Tourenne, C., Polymenidou, M. & Cleveland, D.W. TDP-43 and FUS/TLS: emerging roles in RNA processing and neurodegeneration. *Hum Mol*

bioRxiv preprint doi: https://doi.org/10.1101/789057; this version posted October 1, 2019. The copyright holder for this preprint (which was not certified by peer review) is the author/funder, who has granted bioRxiv a license to display the preprint in perpetuity. It is made available under aCC-BY-NC-ND 4.0 International license.

Genet **19**, R46-64 (2010).

6. Afroz, T. *et al*. Functional and dynamic polymerization of the ALS-linked protein TDP-43 antagonizes its pathologic aggregation. *Nat Commun* **8**, 45 (2017).
7. Shiina, Y., Arima, K., Tabunoki, H. & Satoh, J. TDP-43 dimerizes in human cells in culture. *Cell Mol Neurobiol* **30**, 641-652 (2010).
8. Zhang, Y.J. *et al*. The dual functions of the extreme N-terminus of TDP-43 in regulating its biological activity and inclusion formation. *Hum Mol Genet* **22**, 3112-3122 (2013).
9. Conicella, A.E., Zerze, G.H., Mittal, J. & Fawzi, N.L. ALS Mutations Disrupt Phase Separation Mediated by alpha-Helical Structure in the TDP-43 Low-Complexity C-Terminal Domain. *Structure* **24**, 1537-1549 (2016).
10. Johnson, B.S. *et al*. TDP-43 is intrinsically aggregation-prone, and amyotrophic lateral sclerosis-linked mutations accelerate aggregation and increase toxicity. *J Biol Chem* **284**, 20329-20339 (2009).
11. Watanabe, S., Kaneko, K. & Yamanaka, K. Accelerated disease onset with stabilized familial amyotrophic lateral sclerosis (ALS)-linked mutant TDP-43 proteins. *J Biol Chem* **288**, 3641-3654 (2013).
12. Budini, M. *et al*. Role of selected mutations in the Q/N rich region of TDP-43 in EGFP-12xQ/N-induced aggregate formation. *Brain Res* **1462**, 139-150 (2012).
13. Guenther, E.L. *et al*. Atomic structures of TDP-43 LCD segments and insights into reversible or pathogenic aggregation. *Nat Struct Mol Biol* **25**, 463-471 (2018).
14. Zhang, Y.J. *et al*. Aberrant cleavage of TDP-43 enhances aggregation and cellular toxicity. *Proc Natl Acad Sci U S A* **106**, 7607-7612 (2009).
15. Jiang, L.L. *et al*. The N-terminal dimerization is required for TDP-43 splicing activity. *Sci Rep* **7**, 6196 (2017).
16. Arnold, E.S. *et al*. ALS-linked TDP-43 mutations produce aberrant RNA splicing and adult-onset motor neuron disease without aggregation or loss of nuclear TDP-43. *Proc Natl Acad Sci U S A* **110**, E736-745 (2013).
17. Barmada, S.J. *et al*. Cytoplasmic mislocalization of TDP-43 is toxic to neurons and enhanced by a mutation associated with familial amyotrophic lateral sclerosis. *J Neurosci* **30**, 639-649 (2010).

bioRxiv preprint doi: https://doi.org/10.1101/789057; this version posted October 1, 2019. The copyright holder for this preprint (which was not certified by peer review) is the author/funder, who has granted bioRxiv a license to display the preprint in perpetuity. It is made available under aCC-BY-NC-ND 4.0 International license.

624 18. Ebstein, S.Y., Yagudayeva, I. & Shneider, N.A. Mutant TDP-43 Causes
625 Early-Stage Dose-Dependent Motor Neuron Degeneration in a TARDBP
626 Knockin Mouse Model of ALS. *Cell Rep* **26**, 364-373 e364 (2019).
627 19. Shan, X., Chiang, P.M., Price, D.L. & Wong, P.C. Altered distributions of
628 Gemini of coiled bodies and mitochondria in motor neurons of TDP-43
629 transgenic mice. *Proc Natl Acad Sci U S A* **107**, 16325-16330 (2010).
630 20. Stallings, N.R., Puttaparthi, K., Luther, C.M., Burns, D.K. & Elliott, J.L.
631 Progressive motor weakness in transgenic mice expressing human TDP-43.
632 *Neurobiol Dis* **40**, 404-414 (2010).
633 21. Wegorzewska, I., Bell, S., Cairns, N.J., Miller, T.M. & Baloh, R.H. TDP-43
634 mutant transgenic mice develop features of ALS and frontotemporal lobar
635 degeneration. *Proc Natl Acad Sci U S A* **106**, 18809-18814 (2009).
636 22. White, M.A. *et al*. TDP-43 gains function due to perturbed autoregulation in a
637 Tardbp knock-in mouse model of ALS-FTD. *Nat Neurosci* **21**, 552-563 (2018).
638 23. Wils, H. *et al*. TDP-43 transgenic mice develop spastic paralysis and neuronal
639 inclusions characteristic of ALS and frontotemporal lobar degeneration. *Proc*
640 *Natl Acad Sci U S A* **107**, 3858-3863 (2010).
641 24. Xu, Y.F. *et al*. Wild-type human TDP-43 expression causes TDP-43
642 phosphorylation, mitochondrial aggregation, motor deficits, and early mortality
643 in transgenic mice. *J Neurosci* **30**, 10851-10859 (2010).
644 25. Xu, Y.F. *et al*. Expression of mutant TDP-43 induces neuronal dysfunction in
645 transgenic mice. *Mol Neurodegener* **6**, 73 (2011).
646 26. Braak, H., Ludolph, A.C., Neumann, M., Ravits, J. & Del Tredici, K.
647 Pathological TDP-43 changes in Betz cells differ from those in bulbar and spinal
648 alpha-motoneurons in sporadic amyotrophic lateral sclerosis. *Acta Neuropathol*
649 **133**, 79-90 (2017).
650 27. Shin, Y. *et al*. Spatiotemporal Control of Intracellular Phase Transitions Using
651 Light-Activated optoDroplets. *Cell* **168**, 159-171 e114 (2017).
652 28. Mann, J.R. *et al*. RNA Binding Antagonizes Neurotoxic Phase Transitions of
653 TDP-43. *Neuron* **102**, 321-338 e328 (2019).
654 29. Zhang, P. *et al*. Chronic optogenetic induction of stress granules is cytotoxic and
655 reveals the evolution of ALS-FTD pathology. *Elife* **8** (2019).
656 30. Myers, P.Z. Spinal motoneurons of the larval zebrafish. *J Comp Neurol* **236**,

bioRxiv preprint doi: https://doi.org/10.1101/789057; this version posted October 1, 2019. The copyright holder for this preprint (which was not certified by peer review) is the author/funder, who has granted bioRxiv a license to display the preprint in perpetuity. It is made available under aCC-BY-NC-ND 4.0 International license.

555-561 (1985).

31. Schmid, B. *et al*. Loss of ALS-associated TDP-43 in zebrafish causes muscle degeneration, vascular dysfunction, and reduced motor neuron axon outgrowth. *Proc Natl Acad Sci U S A* **110**, 4986-4991 (2013).

32. Asakawa, K. & Kawakami, K. The Tol2-mediated Gal4-UAS method for gene and enhancer trapping in zebrafish. *Methods* **49**, 275-281 (2009).

33. Taslimi, A. *et al*. An optimized optogenetic clustering tool for probing protein interaction and function. *Nat Commun* **5**, 4925 (2014).

34. Pinarbasi, E.S. *et al*. Active nuclear import and passive nuclear export are the primary determinants of TDP-43 localization. *Sci Rep* **8**, 7083 (2018).

35. Winton, M.J. *et al*. Disturbance of nuclear and cytoplasmic TAR DNA-binding protein (TDP-43) induces disease-like redistribution, sequestration, and aggregate formation. *J Biol Chem* **283**, 13302-13309 (2008).

36. Asakawa, K. & Kawakami, K. Protocadherin-Mediated Cell Repulsion Controls the Central Topography and Efferent Projections of the Abducens Nucleus. *Cell Rep* **24**, 1562-1572 (2018).

37. Santamaria, N., Alhothali, M., Alfonso, M.H., Breydo, L. & Uversky, V.N. Intrinsic disorder in proteins involved in amyotrophic lateral sclerosis. *Cell Mol Life Sci* **74**, 1297-1318 (2017).

38. Austin, J.A. *et al*. Disease causing mutants of TDP-43 nucleic acid binding domains are resistant to aggregation and have increased stability and half-life. *Proc Natl Acad Sci U S A* **111**, 4309-4314 (2014).

39. Klim, J.R. *et al*. ALS-implicated protein TDP-43 sustains levels of STMN2, a mediator of motor neuron growth and repair. *Nat Neurosci* **22**, 167-179 (2019).

40. Scotter, E.L. *et al*. Differential roles of the ubiquitin proteasome system and autophagy in the clearance of soluble and aggregated TDP-43 species. *J Cell Sci* **127**, 1263-1278 (2014).

41. Polymenidou, M. *et al*. Long pre-mRNA depletion and RNA missplicing contribute to neuronal vulnerability from loss of TDP-43. *Nat Neurosci* **14**, 459-468 (2011).

42. Sephton, C.F. *et al*. Identification of neuronal RNA targets of TDP-43-containing ribonucleoprotein complexes. *J Biol Chem* **286**, 1204-1215 (2011).

bioRxiv preprint doi: https://doi.org/10.1101/789057; this version posted October 1, 2019. The copyright holder for this preprint (which was not certified by peer review) is the author/funder, who has granted bioRxiv a license to display the preprint in perpetuity. It is made available under aCC-BY-NC-ND 4.0 International license.

690 43. Tollervey, J.R. *et al*. Characterizing the RNA targets and position-dependent
691 splicing regulation by TDP-43. *Nat Neurosci* **14**, 452-458 (2011).
692 44. Xiao, S. *et al*. RNA targets of TDP-43 identified by UV-CLIP are deregulated in
693 ALS. *Mol Cell Neurosci* **47**, 167-180 (2011).
694 45. Melamed, Z. *et al*. Premature polyadenylation-mediated loss of stathmin-2 is a
695 hallmark of TDP-43-dependent neurodegeneration. *Nat Neurosci* **22**, 180-190
696 (2019).
697 46. Ling, J.P., Pletnikova, O., Troncoso, J.C. & Wong, P.C. TDP-43 repression of
698 nonconserved cryptic exons is compromised in ALS-FTD. *Science* **349**, 650-655
699 (2015).
700 47. Alami, N.H. *et al*. Axonal transport of TDP-43 mRNA granules is impaired by
701 ALS-causing mutations. *Neuron* **81**, 536-543 (2014).
702 48. Bergamin, G., Cieri, D., Vazza, G., Argenton, F. & Mostacciuolo, M.L.
703 Zebrafish Tg(hb9:MTS-Kaede): a new in vivo tool for studying the axonal
704 movement of mitochondria. *Biochim Biophys Acta* **1860**, 1247-1255 (2016).
705 49. Wang, P. *et al*. TDP-43 induces mitochondrial damage and activates the
706 mitochondrial unfolded protein response. *PLoS Genet* **15**, e1007947 (2019).
707 50. Vogler, T.O. *et al*. TDP-43 and RNA form amyloid-like myo-granules in
708 regenerating muscle. *Nature* **563**, 508-513 (2018).
709 51. Laferriere, F. *et al*. TDP-43 extracted from frontotemporal lobar degeneration
710 subject brains displays distinct aggregate assemblies and neurotoxic effects
711 reflecting disease progression rates. *Nat Neurosci* **22**, 65-77 (2019).
712 52. Kawamura, Y., Okazaki, H., O'Brien, P.C. & Dych, P.J. Lumbar motoneurons of
713 man: I) number and diameter histogram of alpha and gamma axons of ventral
714 root. *J Neuropathol Exp Neurol* **36**, 853-860 (1977).
715 53. Mittal, K.R. & Logmani, F.H. Age-related reduction in 8th cervical ventral
716 nerve root myelinated fiber diameters and numbers in man. *J Gerontol* **42**, 8-10
717 (1987).
718 54. Tomlinson, B.E. & Irving, D. The numbers of limb motor neurons in the human
719 lumbosacral cord throughout life. *J Neurol Sci* **34**, 213-219 (1977).
720 55. Piasecki, M., Ireland, A., Jones, D.A. & McPhee, J.S. Age-dependent motor unit
721 remodelling in human limb muscles. *Biogerontology* **17**, 485-496 (2016).
722 56. Telerman-Toppet, N. & Coers, C. Motor innervation and fiber type pattern in

bioRxiv preprint doi: https://doi.org/10.1101/789057; this version posted October 1, 2019. The copyright holder for this preprint (which was not certified by peer review) is the author/funder, who has granted bioRxiv a license to display the preprint in perpetuity. It is made available under aCC-BY-NC-ND 4.0 International license.

amyotrophic lateral sclerosis and in Charcot-Marie-Tooth disease. *Muscle Nerve* **1**, 133-139 (1978).

57. Asakawa, K. *et al*. Genetic dissection of neural circuits by Tol2 transposon-mediated Gal4 gene and enhancer trapping in zebrafish. *Proc Natl Acad Sci U S A* **105**, 1255-1260 (2008).

58. Asakawa, K., Abe, G. & Kawakami, K. Cellular dissection of the spinal cord motor column by BAC transgenesis and gene trapping in zebrafish. *Front Neural Circuits* **7**, 100 (2013).

59. Moreno-Mateos, M.A. *et al*. CRISPRscan: designing highly efficient sgRNAs for CRISPR-Cas9 targeting in vivo. *Nat Methods* **12**, 982-988 (2015).

60. Asakawa, K. & Kawakami, K. A transgenic zebrafish for monitoring in vivo microtubule structures. *Dev Dyn* **239**, 2695-2699 (2010).

Figure legends

Figure 1

Overexpression of TDP-43 halts axon outgrowth independently of cytoplasmic TDP-43 aggregation. (A, B) CaPs (arrows) in Tg[SAIG213A] Tg[UAS:EGFP] fish. Orange, black and grey arrowheads indicate dorsal and ventral limits of the spinal cord, and ventral myotomal borders, respectively. (C) CaPs in Tg[SAIG213A] Tg[UAS:EGFP] (left) and Tg[SAIG213A] Tg[UAS:EGFP] Tg[UAS:mRFP1-TDP-43z] (right) larvae at 48 hpf. The structure of Tg[UAS:mRFP1-TDP-43z] transgene (bottom). (D) The lateral and frontal views of skeletonized CaP axons of Tg[SAIG213A] Tg[UAS:EGFP] (left) and Tg[SAIG213A] Tg[UAS:EGFP] Tg[UAS:mRFP1-TDP-43z] (right). The axon branch points and terminals are indicated by red and green, respectively. (See also Sup Movie1). (E, F) Total length and branching frequency of CaP axons at the spinal segment 14-17 of Tg[SAIG213A] Tg[UAS:EGFP] (green, 12 CaPs, 5 animals) and Tg[SAIG213A] Tg[UAS:EGFP] Tg[UAS:mRFP1-TDP-43z] (mageneta, 12 CaPs, 6 animals). *, $p < 0.0001$. NS, Not statistically significant. (G) Localization of mRFP1-TDP-43z in a CaP of Tg[SAIG213A] Tg[UAS:Gtuba2]

bioRxiv preprint doi: https://doi.org/10.1101/789057; this version posted October 1, 2019. The copyright holder for this preprint (which was not certified by peer review) is the author/funder, who has granted bioRxiv a license to display the preprint in perpetuity. It is made available under aCC-BY-NC-ND 4.0 International license.

Tg[UAS:mRFP1-TDP-43z] at 48 hpf. EGFP-taggedαtubulin expressed from Tg[UAS:Gtuba2] [60] serves as a marker for cytoplasm. The bars indicate 20 μm (B, C), 40 μm (D), 2 μm (G).

Figure 2

A photo-switchable TDP-43: opTDP-43. (A) The structures of Tg[UAS:mRFP1-CRY2olig] and Tg[UAS:opTDP-43z]. (B) Tg[SAIG213A] Tg[UAS:mRFP1-CRY2olig] fish at 30 hpf. A montage of a CaP expressing mRFP1-CRY2olig (boxed). The blue light was illuminated from 0 to 30 min. (C) Tg[SAGFF73A] Tg[UAS:opTDP-43z] fish at 28 hpf (0 min) and 31.5 hpf (210 hpf). A montage of a skeletal muscle cell expressing opTDP-43z (dashed box). The blue light was illuminated from 0 to 210 min. (D, E) The averaged change of opTDP-43 intensity in the cytoplasm (D) and nucleus (E) during the illumination (N = 8 cells). The asterisks indicate the emergence of statistically significant change in opTDP-43 fluorescence intensity in comparison to the opTDP-43 level at t = 0 ($p < 0.05$, t test). (F) Immunofluorescence of the skeletal muscle of the fish illuminated for 3.5 hours, using anti-RFP antibody (for opTDP-43) and anti-ubiquitin antibodies. Arrows indicate the representative of opTDP-43 droplets that are partially ubiquitinated. N, nucleus. The bars indicate 500 bp (A), 20 μm (B, C left), 10 μm (C right), and 2 μm (F).

Figure 3

Light illumination-dependent cytoplasmic mislocalization of opTDP-43 in neuronal cells. (A) The dorsal view of the spinal cord at the segment 14 -17 levels of a Tg[SAIG213A] Tg[mnr2b-hs:Gal4] Tg[UAS:opTDP-43z] Tg[UAS:EGFP] quadruple transgenic fish. Two spinal motor neurons (M1 and M2) and a Rohon-Beard sensory neuron (RB cell, S) highlighted with dashed boxes were analyzed in detail in B and C. (B, C) A montage of two spinal motor neurons (M1 and M2 in A) and a RB cell during the light illumination. The graphs show the fluorescent intensities of opTDP-43 along

bioRxiv preprint doi: https://doi.org/10.1101/789057; this version posted October 1, 2019. The copyright holder for this preprint (which was not certified by peer review) is the author/funder, who has granted bioRxiv a license to display the preprint in perpetuity. It is made available under aCC-BY-NC-ND 4.0 International license.

781 the dotted line drawn from the lateral (L) to medial edge (M) of the EGFP signal. The
782 blue arrows indicate the cytoplasmic increase of opTDP-43. The bars indicate 20 μm
783 (A), 10 μm (B).
784
785 **Figure 4**
786 **The light-dependent transient cytoplasmic mislocalization of opTDP-43z is**
787 **accompanied by diminished motor axon outgrowth.** (A) The light-illumination
788 paradigm of CaPs. The spinal cord of Tg[SAIG213A] Tg[UAS:opTDP-43z]
789 Tg[UAS:EGFP] fish at the spinal segment 13-18 level were illuminated with a blue
790 laser, and CaPs were subjected to morphological analysis at 48-50 hpf. Shown images
791 are a single CaP from dorsal (28 and 31 hpf) and lateral (48 hpf) views. The
792 fluorescence intensity along the longest inner diameter (dashed magenta line) is plotted
793 at each time point. Blue arrows indicate the presumptive cytoplasm area, where the
794 opTDP-43z signal is faint. (B) Cytoplasmic shift of opTDP-43 localization is evaluated
795 as a relative value of minimal (*F*min, cytoplasm) and maximal (*F*max, nuclear)
796 fluorescence intensity along the longest inner diameter (dashed magenta line). The
797 results were obtained from 32 cells (28 and 31 hpf) and 17 cells (48 hpf) in three
798 independent Tg[SAIG213A] Tg[UAS:opTDP-43z] Tg[UAS:EGFP] fish. * $p < 0.0001$ (t
799 test). (C) CaP motor axons with (BL) or without (Dark) blue light stimulation. (D, E)
800 The total axon length and branching frequency of CaP motor axons in Tg[SAIG213A]
801 Tg[UAS:EGFP] fish raised under normal laboratory light-dark cycle (L/D, the
802 overlapping data sets with Figure 1E, F), Tg[SAIG213A] Tg[UAS:opTDP-43z]
803 Tg[UAS:EGFP] fish with (BL, 15 cells, 4 animals) or without (Da, 15 cells, 4 animals)
804 blue light stimulation, and Tg[SAIG213A] Tg[UAS:mRFP1-CRY2olig]
805 Tg[UAS:EGFP] fish with the blue light stimulation (7 cells, 2 animals). ** $p = 0.0068$ (t
806 test). NS, not significant. (I, J) Somas of the CaPs (arrowhead) and other
807 *mnr2b*-positive spinal motor neurons in the spinal segment 14 (I) and 13-17 (J) of
808 Tg[SAIG213A] Tg[UAS:opTDP-43z] Tg[mnr2b-hs:EGFP-TDP43z] fish that was

bioRxiv preprint doi: https://doi.org/10.1101/789057; this version posted October 1, 2019. The copyright holder for this preprint (which was not certified by peer review) is the author/funder, who has granted bioRxiv a license to display the preprint in perpetuity. It is made available under aCC-BY-NC-ND 4.0 International license.

809 illuminated with a blue light during 28 hpf- 32 hpf. (K, L) Evaluation of cytoplasmic
810 shift of opTDP-43z and EGFP-TDP-43z in the CaP in I. (K) The fluorescence
811 intensities of opTDP-43z (magenta) and EGFP-TDP-43z (green) was plotted along the
812 blue dashed arrows. Images shown are over enhanced for identification of soma outline.
813 (L) The relative intensity of cytoplasmic signal (*F*min/*F*max) for opTDP-43z (magenta)
814 and for EGFP-TDP-43z (green) in each spinal segment. The bars indicate 5 μm (A, B),
815 20 μm (C, J), 10 μm (I).
816
817 **Figure 5**
818 **Axonal shrinkage and myofiber denervation caused by light stimulation of**
819 **opTDP-43z.**
820 (A) A CaP motor axon in Tg[SAIG213A] Tg[UAS:EGFP] fish. DCCT (green box) was
821 magnified on the right. Primary, secondary and tertial branchings were indicated in red.
822 (B) Light-illumination paradigm. (C, D, E) Total length (C), growth rate (D) and
823 population change in axon terminal number (E) of DCCTs in Tg[SAIG213A]
824 Tg[UAS:EGFP] Tg[UAS:opTDP-43z] fish (Dark: 29 cells, 5 animals, BL: 18 cells, 3
825 animals) and Tg[SAIG213A] Tg[UAS:EGFP] fish raised under normal dark light
826 cycles (D/L: 17 cells, 3 animals). *, p = 0.0224 (t test). (F) The lateral view of the trunk
827 of Tg[SAIG213A] Tg[UAS:V2V] Tg[actc1b:tdT-chrnd] fish (left) and neuromuscular
828 synapses of the DCCT (right) at 56 hpf. The dashed yellow lines indicate the CaP axon
829 shaft. (G) Neuromuscular synapses of the DCCT in Tg[SAIG213A]
830 Tg[UAS:opTDP-43z] Tg[UAS:V2V] Tg[actc1b:tdT-chrnd] fish at 56 hpf. (H, I) Live
831 imaging of DCCT neuromuscular synapses. Yellow arrowheads indicate the
832 neuromuscular synapses that were not present at 72 hpf. The yellow dashed lines, dots,
833 arrows indicate axon shafts, primary branching points, and contact sites with the
834 myotomal boundaries of CaPs, respectively. In I, Z-stacks are produced from
835 3D-rotated images made by Imaris, to make the denervation events (arrowhead) clearly
836 visible. The bars indicate 10 μm (A top, F right), 50 μm (A bottom, F left), 5μm (H).

bioRxiv preprint doi: https://doi.org/10.1101/789057; this version posted October 1, 2019. The copyright holder for this preprint (which was not certified by peer review) is the author/funder, who has granted bioRxiv a license to display the preprint in perpetuity. It is made available under aCC-BY-NC-ND 4.0 International license.

Figure 6

Long-term light stimulation of opTDP-43h induces TDP-43 aggregation that seeds non-optogenetic TDP-43 aggregation

(A) Chronic field illumination of unrestrained larvae from 2 dpf -5 dpf. (B, C) Live imaging of the spinal motor column of Tg[mnr2b-hs:EGFP-TDP43z] Tg[mnr2b-hs:opTDP-43h] (B) and Tg[mnr2b-hs:EGFP-TDP43z] Tg[mnr2b-hs:opTDP-43h^{A315T}] (C) fish from 2 - 5 dpf. (D) Chronically light-stimulated opTDP-43h (left) and opTDP-43h^{A315T} (right) aggregates in the cytoplasm and seed EGFP-TDP-43z aggregation. Arrowheads indicate opTDP-43 and opTDP-43h^{A315T} aggregates that contain EGFP-TDP-43z. (E) RT-PCR analysis for opTDP-43h (opT43h) and opTDP-43h^{A315T} (A315T). cDNA samples were extracted from Tg[mnr2b-hs:EGFP-TDP43z] (none), Tg[mnr2b-hs:EGFP-TDP43z] Tg[mnr2b-hs:opTDP-43h] (opT43h), and Tg[mnr2b-hs:EGFP-TDP43z] Tg[mnr2b-hs:opTDP-43h^{A315T}] (A315T) larvae at 72hpf. EGFP and zfand5b are internal controls. (F, G, H) Longitudinal single cell analyses of opTDP-43h or opTDP-43h^{A315T} fluorescence intensity (RFP) relative to EGFP-TDP-43z (GFP) (64 cells from 4 animals, for each). * $p < 0.001$ (t test). ** $p = 0.03$ (t test). (I) Failure rate of swimming bladder (SB) inflation of Tg[mnr2b-hs:EGFP-TDP43z] (none), Tg[mnr2b-hs:EGFP-TDP43z] Tg[mnr2b-hs:opTDP-43h] (opT43h), and Tg[mnr2b-hs:EGFP-TDP43z] Tg[mnr2b-hs:opTDP-43h^{A315T}] (A315T) larvae at 5 dpf. Figures indicate the number of illuminated fish examined. SB inflation failure was not observed when fish were raised under normal dark light cycles ($N > 100$ for each). The bars indicates 20 μm (B) and 5 μm (D).

Figure 7

Sequentially regulated illumination-triggered TDP-43 Knot and Aggregate formation

bioRxiv preprint doi: https://doi.org/10.1101/789057; this version posted October 1, 2019. The copyright holder for this preprint (which was not certified by peer review) is the author/funder, who has granted bioRxiv a license to display the preprint in perpetuity. It is made available under aCC-BY-NC-ND 4.0 International license.

In physiological conditions, TDP-43 forms oligomers via its N-terminus and is primarily localized in the nucleus. Spinal motor neurons keep cytoplasmic concentration of TDP-43 oligomers at a low level to prevent them from turning into toxic irreversible oligomers mediated by the C-terminus IDRs (toxic "knots"), which possess competence for developing into pathological TDP-43 aggregates, a hallmark of ALS. CRY2olig-driven opTDP-43 oligomerization promotes pathological change of the motor neurons, such as axon retraction associated with myofiber denervation, prior to accumulation of distinct cytoplasmic aggregates. Whether CRY2olig-diriven opTDP-43 aggregates are toxic to the motor neurons and whether CRY2olig-diriven aggregates eventually deplete endogenous nuclear TDP-43 pools are unknown.

Supplementary Figure 1

Functional validation of opTDP-43z using TDP-43 knockout fish.

(A) The structure of human and zebrafish Tardbp/TDP-43 proteins. RRM, RNA-recognition motif. IDR, Intrinsically disordered region (B, C) The *tardbp-n115* and *tardbpl-n94* mutations are frame-shift deletions that cause protein truncation. The deleted nucleotides were indicated by red lower cases. The grey bars indicate ectopically added peptide due to the frame shift. (D) The lateral views of the wild type (top) and double homozygous (bottom) larvae at 48 hpf. The arrow and arrowhead indicate the swollen heart and the stacked red blood cells on the far side of the yolk, respectively. (E) Rescue rate of the blood circulation defect of the *tardbp-n115* *tardbpl-n94* homozygotes (DKOs). The numbers on the histograms show the total numbers of DKOs investigated obtained from three independent microinjection experiments for each TDP-43 construct.

Supplementary Figure 2

Whole-body overexpression of mRFP1-TDP-43z is toxic to zebrafish.

bioRxiv preprint doi: https://doi.org/10.1101/789057; this version posted October 1, 2019. The copyright holder for this preprint (which was not certified by peer review) is the author/funder, who has granted bioRxiv a license to display the preprint in perpetuity. It is made available under aCC-BY-NC-ND 4.0 International license.

892 The lateral view of Tg[SAGFF73] (top) and Tg[SAGFF73] Tg [UAS:mRFP1-TDP-43z]
893 (bottom) embryos at 24 hpf. The RFP signal is shown in the right panel.
894
895 **Supplementary Figure 3**
896 **Cell-type specificity of light-dependent cytoplasmic opTDP-43z mislocalization.**
897 (A) The nuclear-enriched opTDP-43z localization was not changed by the 3-hour blue
898 light illumination in the embryonic epithelial cells. (B) opTDP-43z localization was not
899 changed by the 4-hour blue light illumination in the differentiated skeletal muscle cells.
900 Cytoplasmic opTDP-43 droplets were occasionally observed independently of light
901 illumination. These light-insensitive opTDP-43 droplets were static throughout the
902 experiment.
903
904 **Supplementary Movie 1**
905 The skeletonized CaP axons of Tg[SAIG213A] Tg[UAS:EGFP] (left) and
906 Tg[SAIG213A] Tg[UAS:EGFP] Tg[UAS:mRFP1-TDP-43z] (right). The axon branch
907 points and terminals are indicated by red and green, respectively.
908
909 **Supplementary Movie 2**
910 The lateral view of CaPs of Tg[SAIG213A] Tg[UAS:mRFP1-CRY2olig] double
911 transgenic embryo. The blue light was illuminated from 0 to 30 min (indicated by a blue
912 dot).
913
914 **Supplementary Movie 3**
915 Skeletal muscle cells expressing opTDP-43z opTDP-43z illuminated with blue light in
916 in Tg[SAGFF73A] Tg[UAS:opTDP-43z] fish at 28 hpf.
917
918 **Supplementary Movie 4**

bioRxiv preprint doi: https://doi.org/10.1101/789057; this version posted October 1, 2019. The copyright holder for this preprint (which was not certified by peer review) is the author/funder, who has granted bioRxiv a license to display the preprint in perpetuity. It is made available under aCC-BY-NC-ND 4.0 International license.

919 The dorsal view of the spinal cord at the segment 14 -17 levels of a Tg[SAIG213A]
920 Tg[mnr2b-hs:Gal4] Tg[UAS:opTDP-43z] Tg[UAS:EGFP] quadruple transgenic fish.
921 EGFP (left) and opTDP-43z (right) were presented side by side. The transverse planes
922 for EGFP and opTDP-43z signals are not completely matched because they are
923 independently registered using Image J software.
924
925 **Supplementary Movie 5**
926 A Tg[mnr2b-hs:EGFP-TDP43z] Tg[mnr2b-hs:opTDP-43h^{A315T}] (A315T) larva
927 (focused) that had been illuminated with blue light during 2-5 dpf is lying at the bottom
928 of the dish with normal heart beat but without the swim bladder inflation. Its sibling
929 (Tg[mnr2b-hs:EGFP-TDP43z] larva) that experienced the same illumination procedure
930 is capable of swimming freely with an inflated swim bladder. The movie is played in
931 actual speed.
932

bioRxiv preprint doi: https://doi.org/10.1101/789057; this version posted October 1, 2019. The copyright holder for this preprint (which was not certified by peer review) is the author/funder, who has granted bioRxiv a license to display the preprint in perpetuity. It is made available under aCC-BY-NC-ND 4.0 International license.

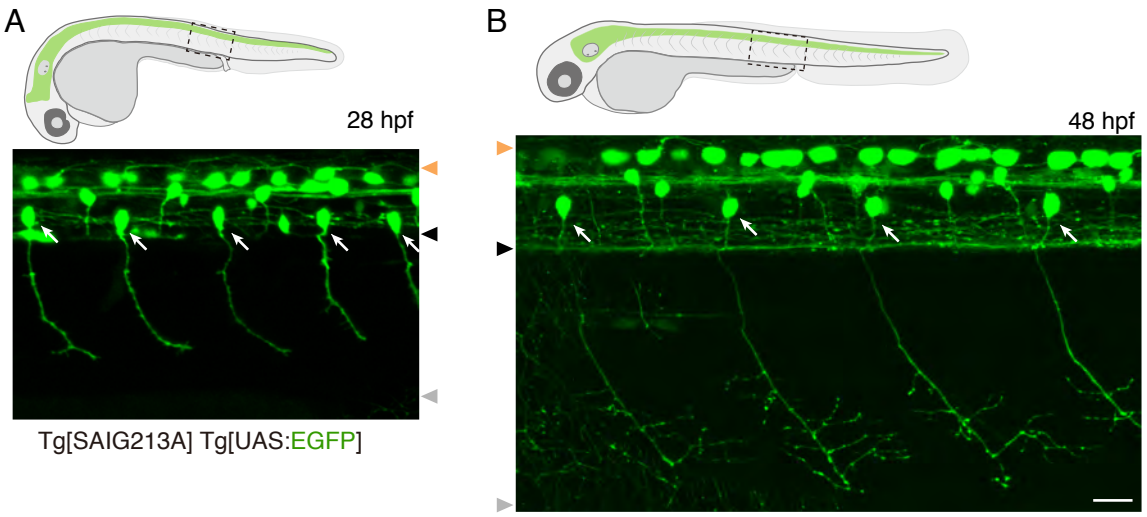

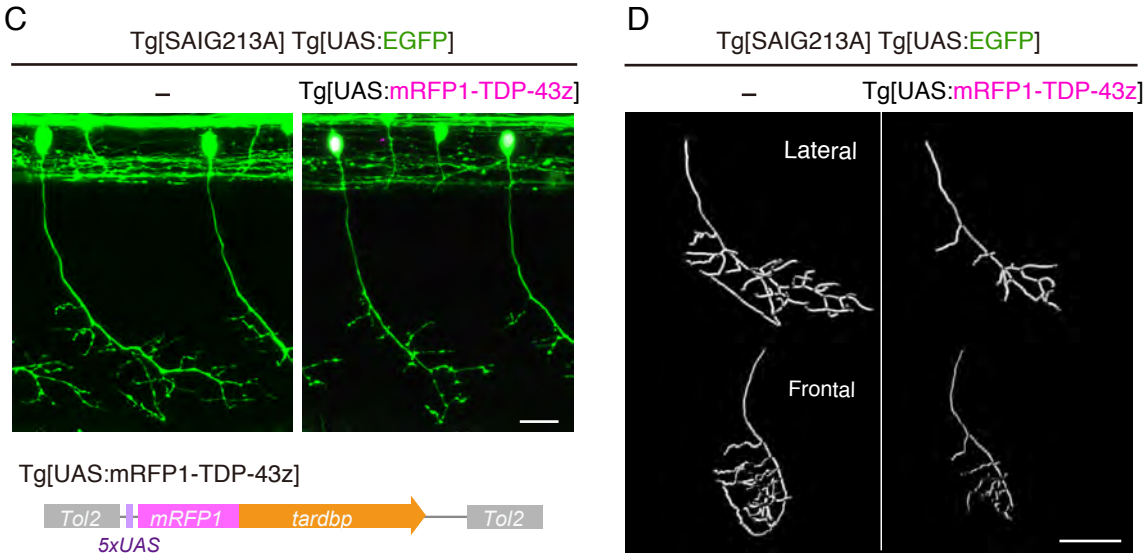

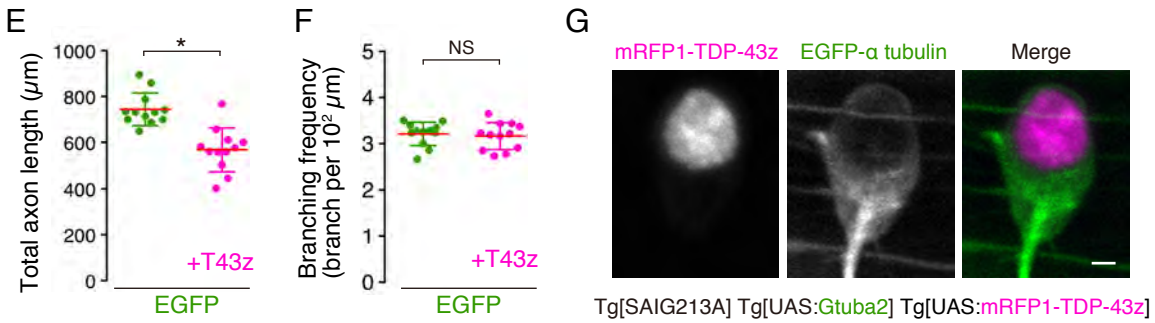

bioRxiv preprint doi: https://doi.org/10.1101/789057; this version posted October 1, 2019. The copyright holder for this preprint (which was not certified by peer review) is the author/funder, who has granted bioRxiv a license to display the preprint in perpetuity. It is made available under aCC-BY-NC-ND 4.0 International license.

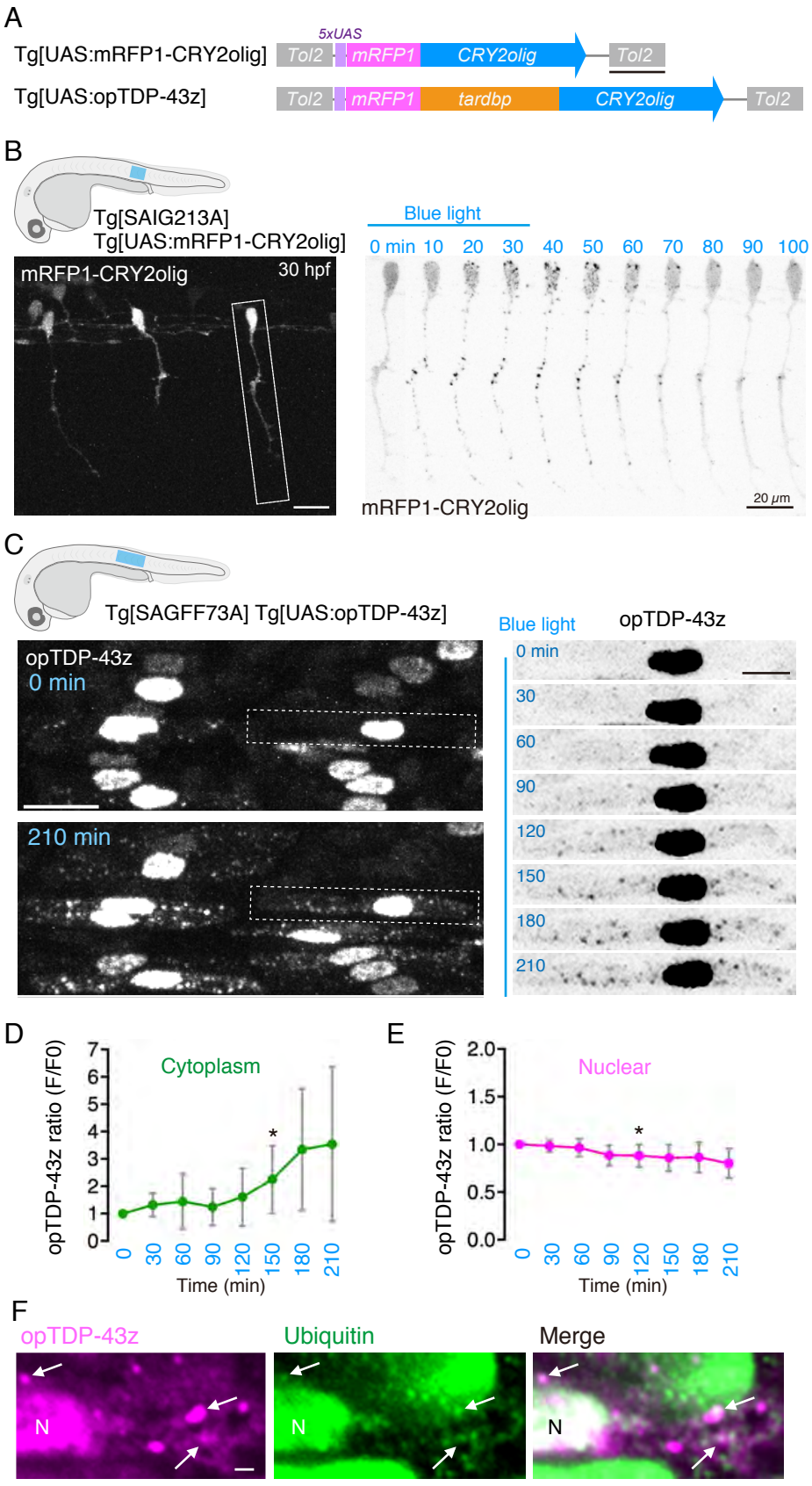

Asakawa et al. Figure 2

bioRxiv preprint doi: https://doi.org/10.1101/789057; this version posted October 1, 2019. The copyright holder for this preprint (which was not certified by peer review) is the author/funder, who has granted bioRxiv a license to display the preprint in perpetuity. It is made available under aCC-BY-NC-ND 4.0 International license.

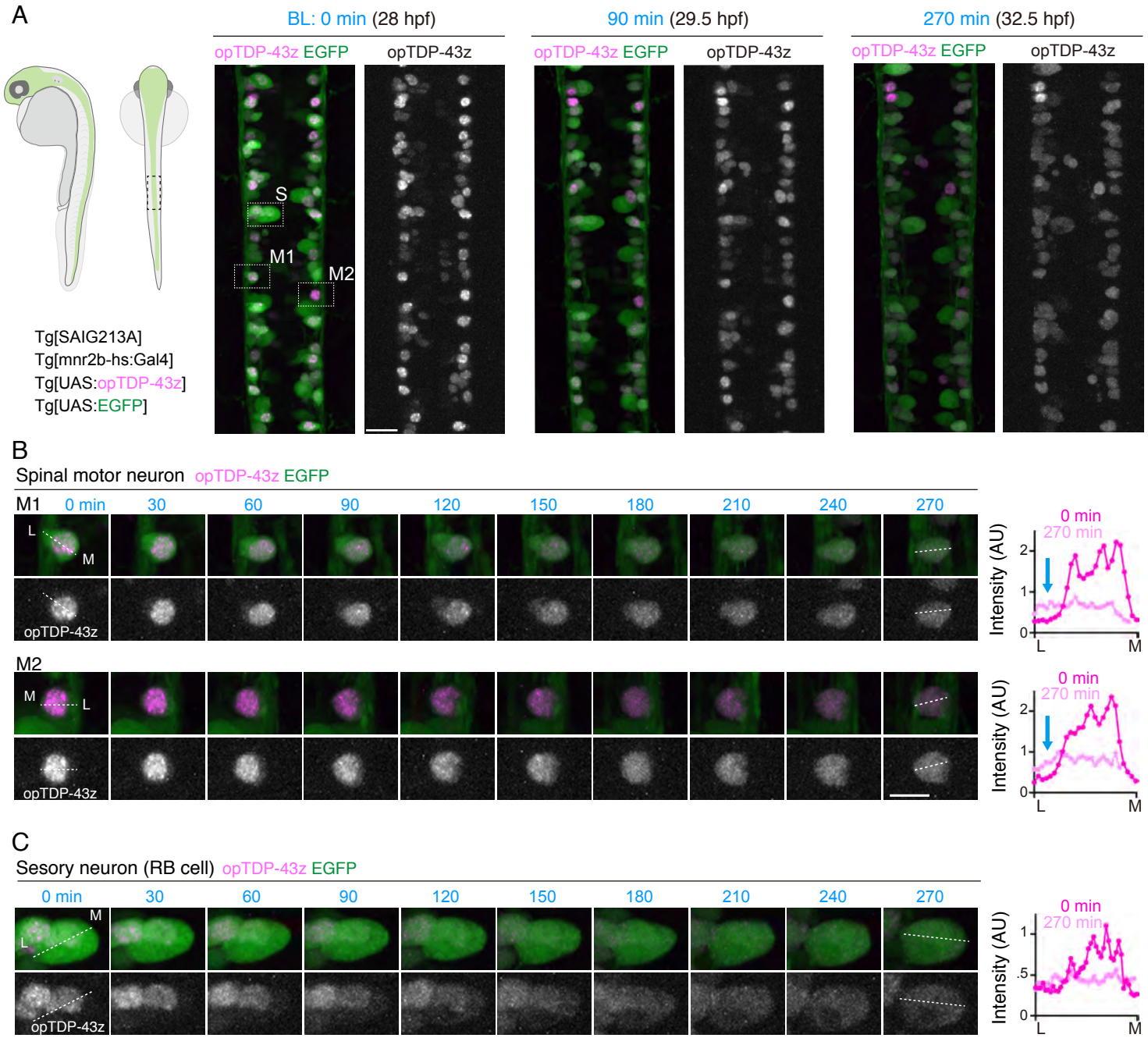

Asakawa et al. Figure 3

bioRxiv preprint doi: https://doi.org/10.1101/789057; this version posted October 1, 2019. The copyright holder for this preprint (which was not certified by peer review) is the author/funder, who has granted bioRxiv a license to display the preprint in perpetuity. It is made available under aCC-BY-NC-ND 4.0 International license.

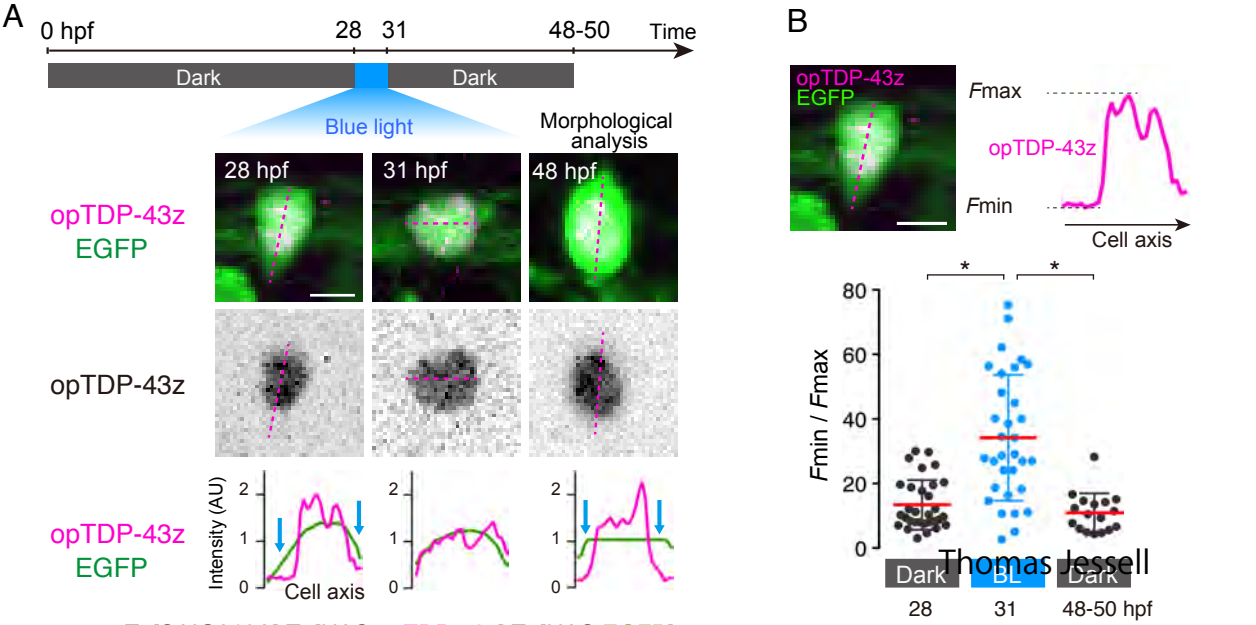

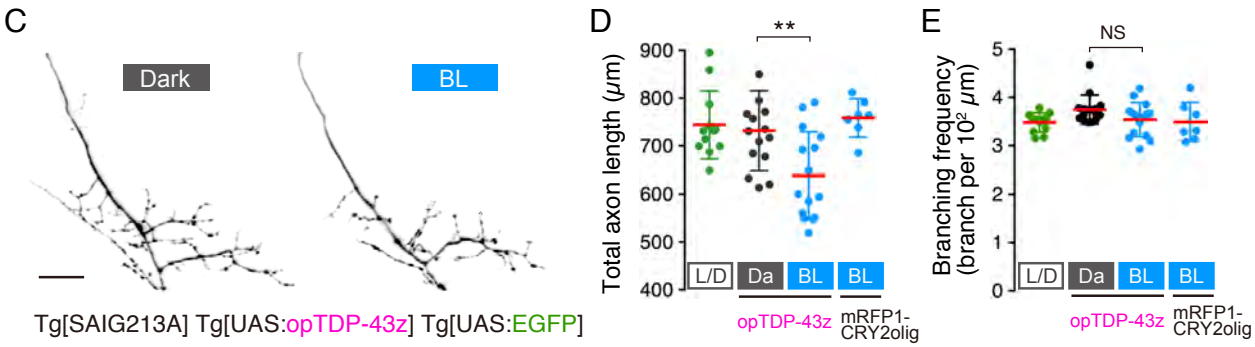

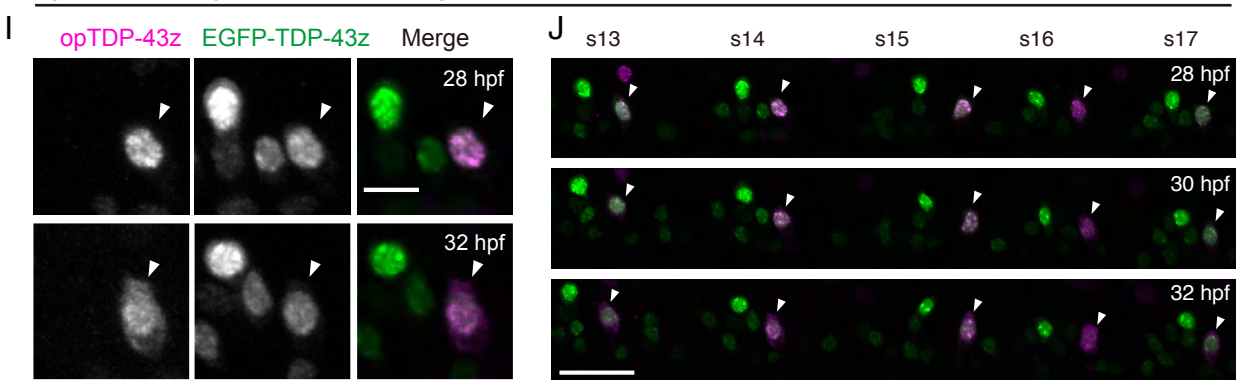

bioRxiv preprint doi: https://doi.org/10.1101/789057; this version posted October 1, 2019. The copyright holder for this preprint (which was not certified by peer review) is the author/funder, who has granted bioRxiv a license to display the preprint in perpetuity. It is made available under aCC-BY-NC-ND 4.0 International license.

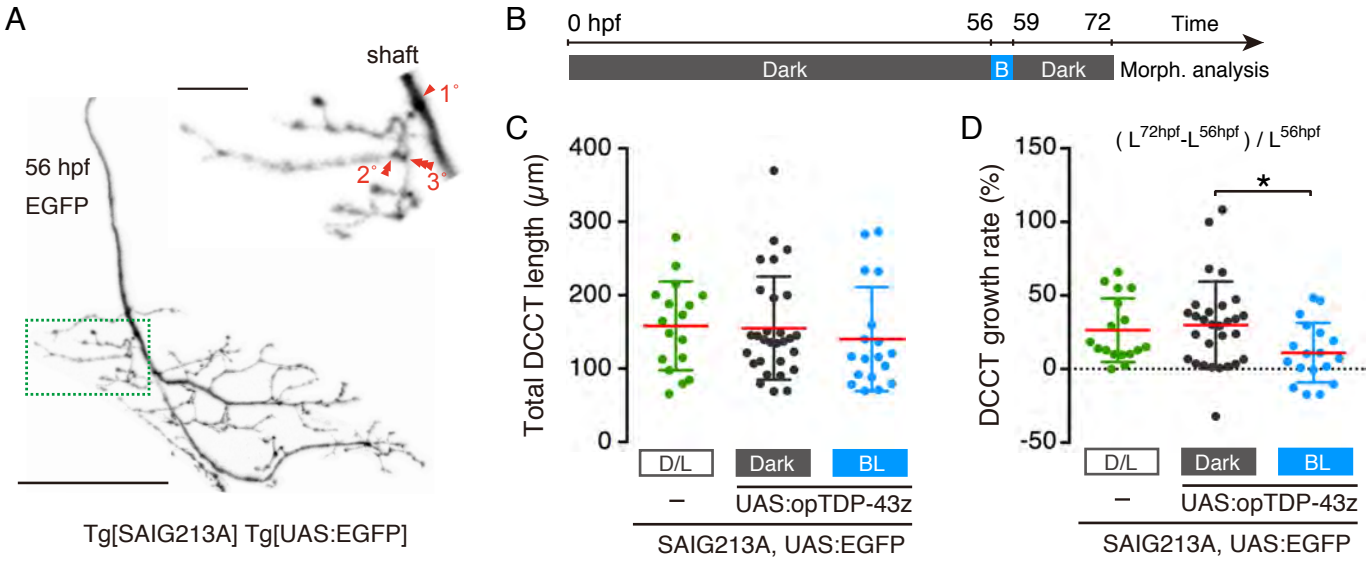

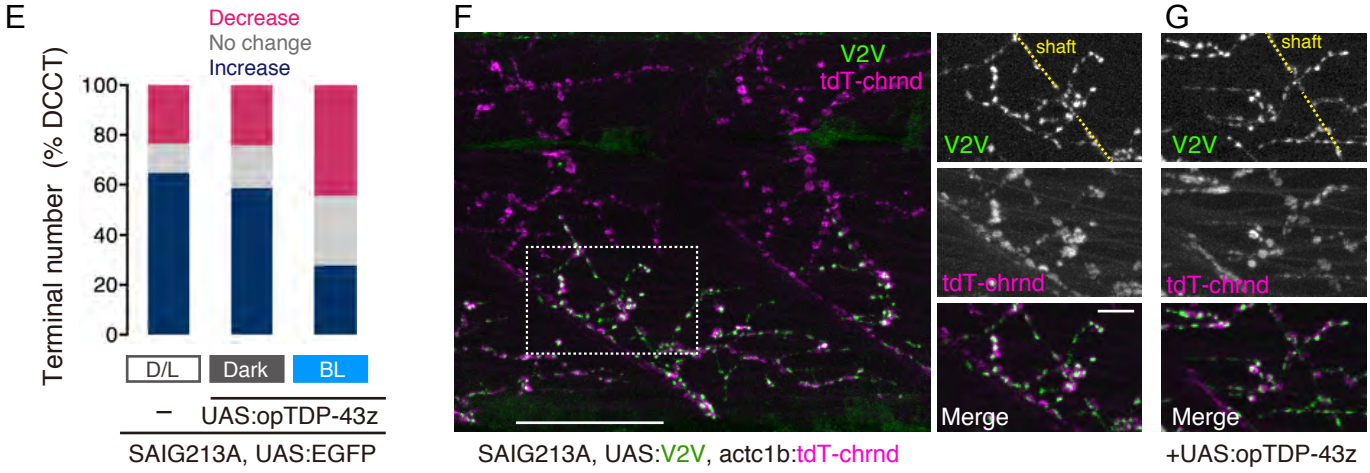

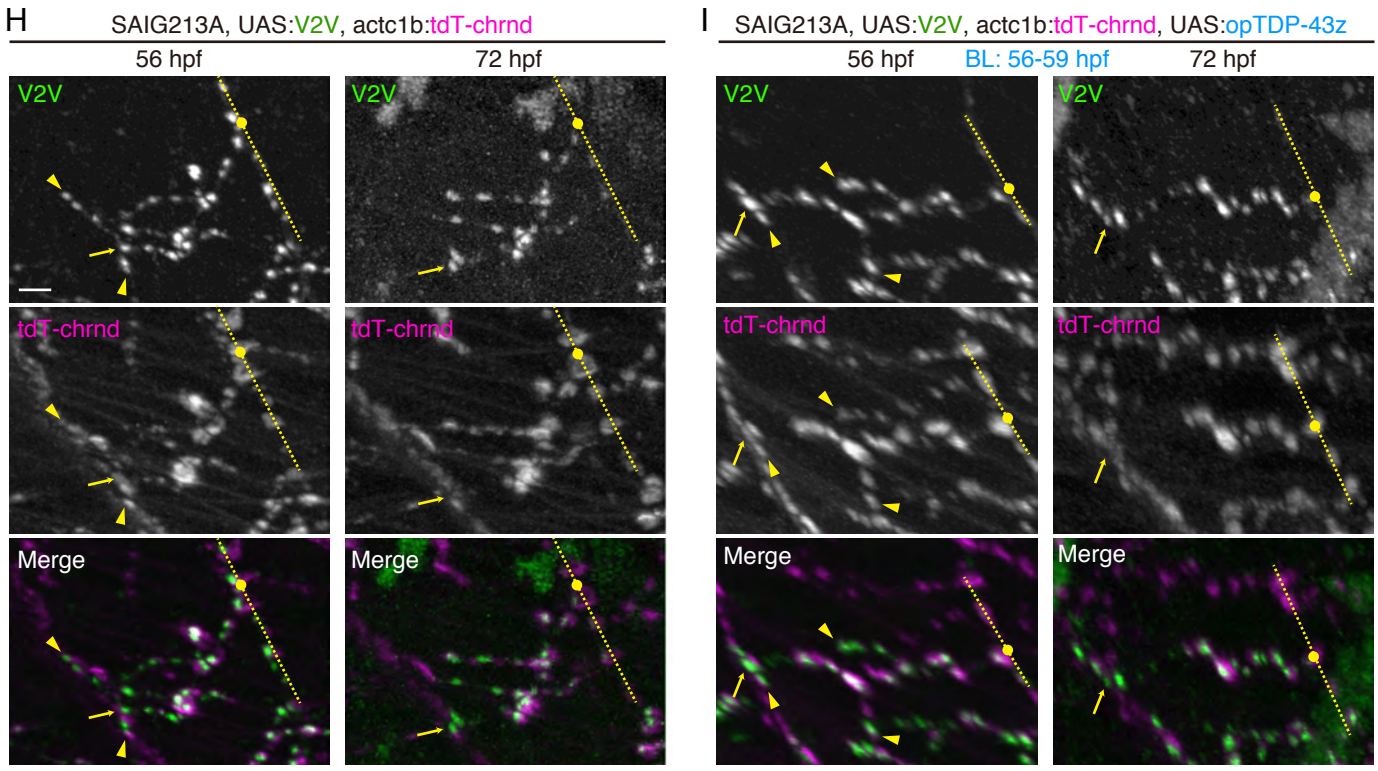

bioRxiv preprint doi: https://doi.org/10.1101/789057; this version posted October 1, 2019. The copyright holder for this preprint (which was not certified by peer review) is the author/funder, who has granted bioRxiv a license to display the preprint in perpetuity. It is made available under aCC-BY-NC-ND 4.0 International license.

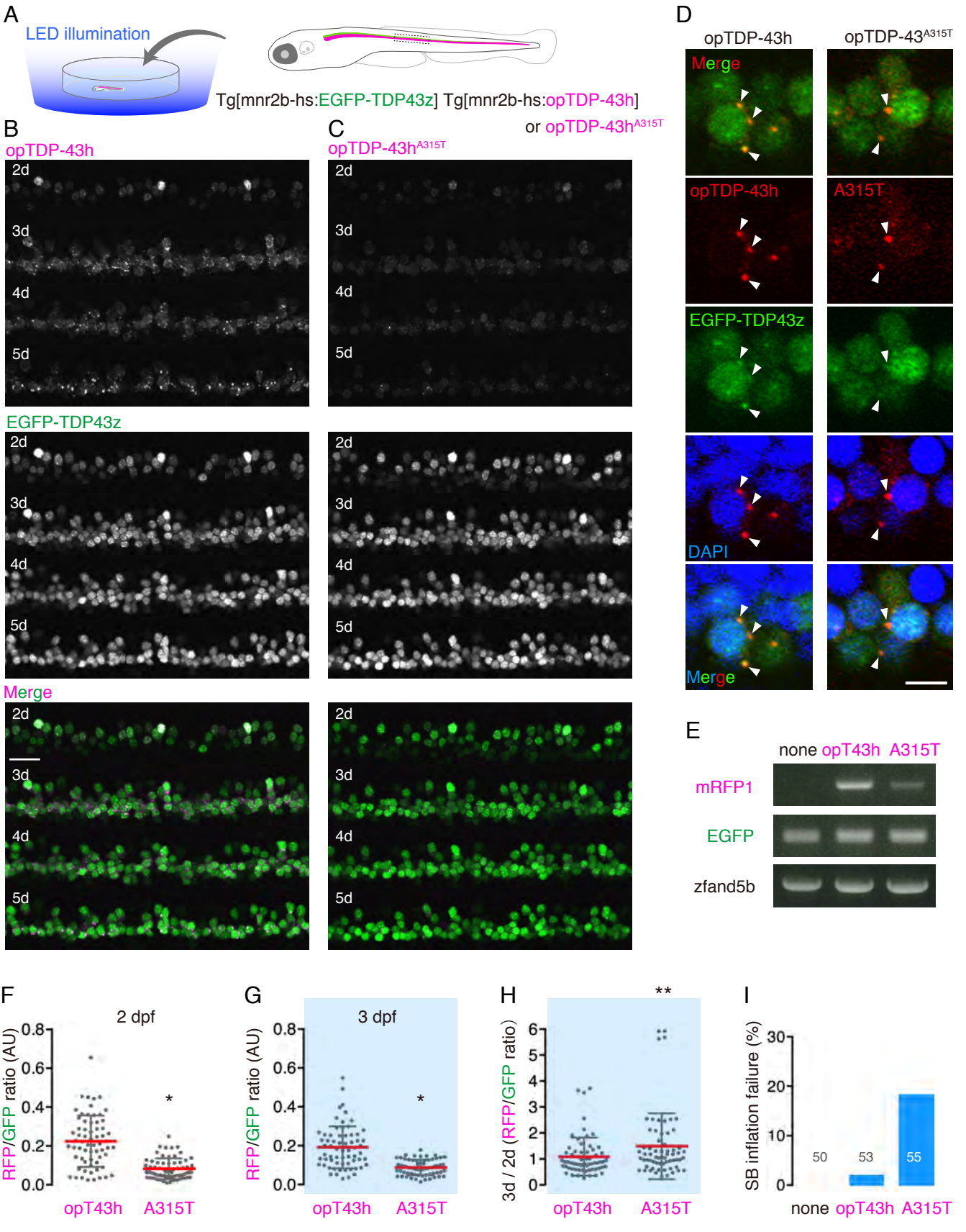

Asakawa et al. Figure 6

bioRxiv preprint doi: https://doi.org/10.1101/789057; this version posted October 1, 2019. The copyright holder for this preprint (which was not certified by peer review) is the author/funder, who has granted bioRxiv a license to display the preprint in perpetuity. It is made available under aCC-BY-NC-ND 4.0 International license.

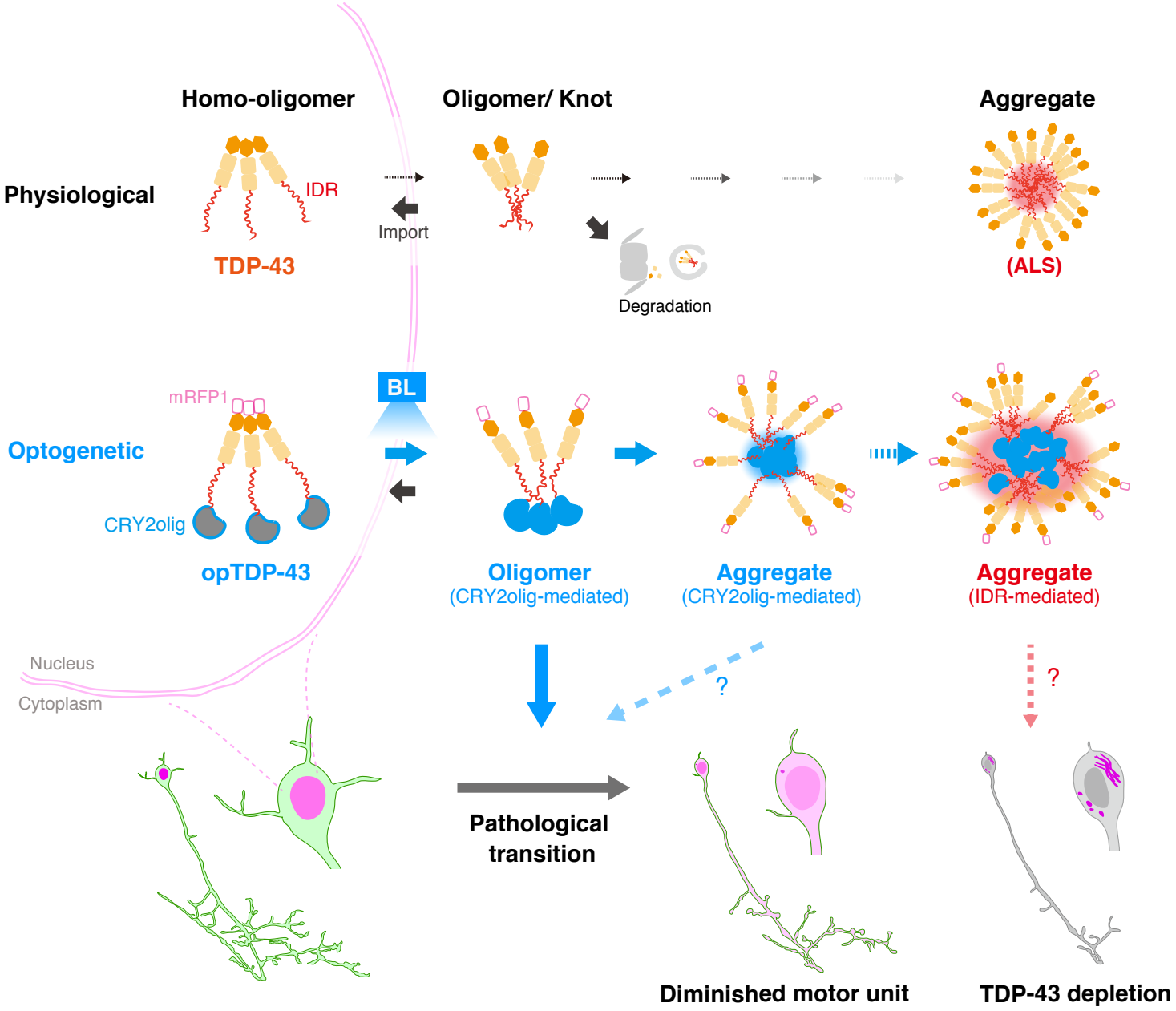

Asakawa et al. Figure 7

bioRxiv preprint doi: https://doi.org/10.1101/789057; this version posted October 1, 2019. The copyright holder for this preprint (which was not certified by peer review) is the author/funder, who has granted bioRxiv a license to display the preprint in perpetuity. It is made available under aCC-BY-NC-ND 4.0 International license.

A

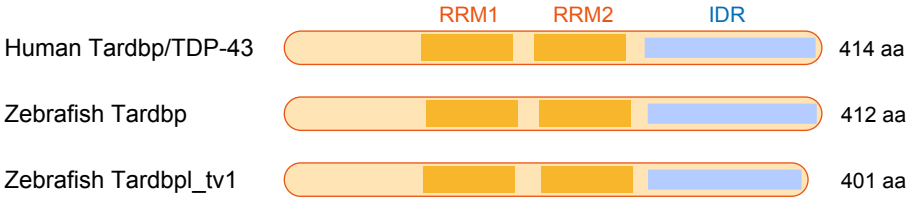

B

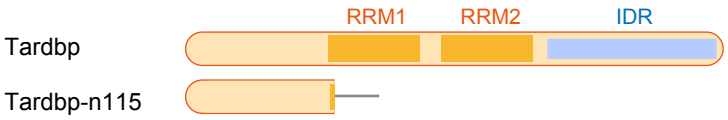

GTG CT [gggtctgccatggaagacttcagagcaagacttaaaagactact] T CGG TAC ATT TGG GGA AGT CAT CAT GGT GCA GGT CAA GCG GGA TGT GAA GAC AGG AAA TTC AAA AGG GTT TGG CTT TGT GAG GTT TGG AGA CTG GGA GAC TCA GAG TAA GGT ... (Deletion: 345~388)

C

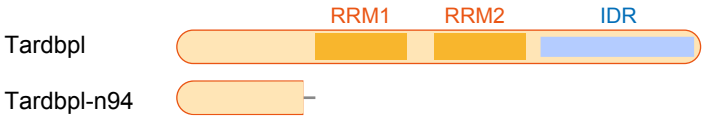

GCA TCG GC [ggtgaagatcaagaggggc] A TCC AGA AGA CAT CAG ATT TGA TTG ... (Deletion: 282~300)

D

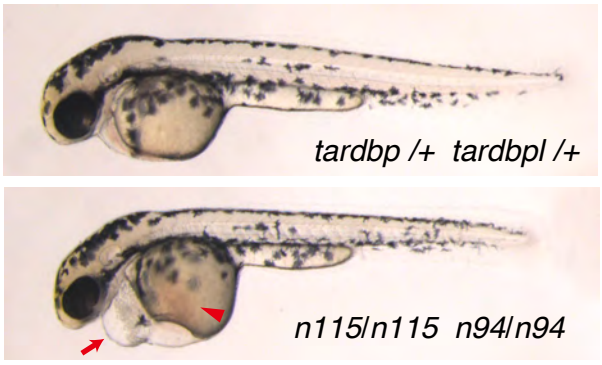

E

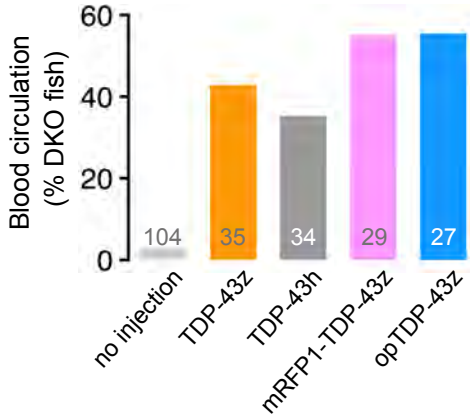

Asakawa et al. Figure S1

bioRxiv preprint doi: https://doi.org/10.1101/789057; this version posted October 1, 2019. The copyright holder for this preprint (which was not certified by peer review) is the author/funder, who has granted bioRxiv a license to display the preprint in perpetuity. It is made available under aCC-BY-NC-ND 4.0 International license.

Tg[SAGFF73A]

Tg[SAGFF73A]
Tg[UAS:mRFP1-TDP-43z]

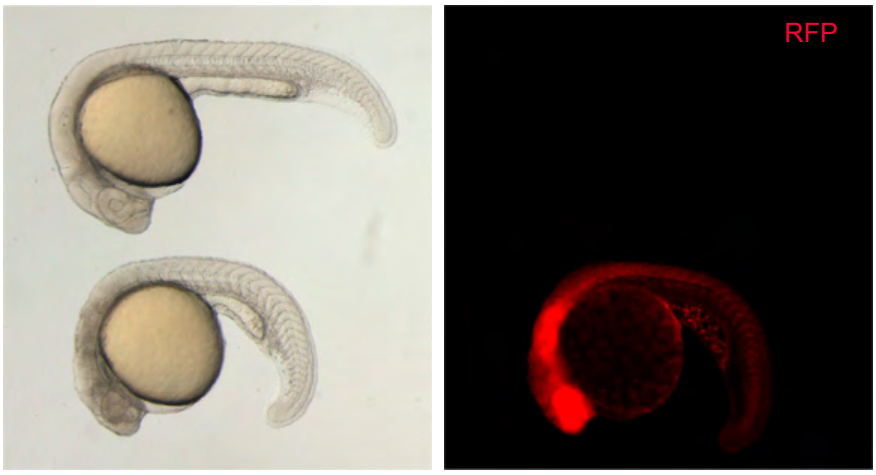

Asakawa et al. Figure S2

bioRxiv preprint doi: https://doi.org/10.1101/789057; this version posted October 1, 2019. The copyright holder for this preprint (which was not certified by peer review) is the author/funder, who has granted bioRxiv a license to display the preprint in perpetuity. It is made available under aCC-BY-NC-ND 4.0 International license.

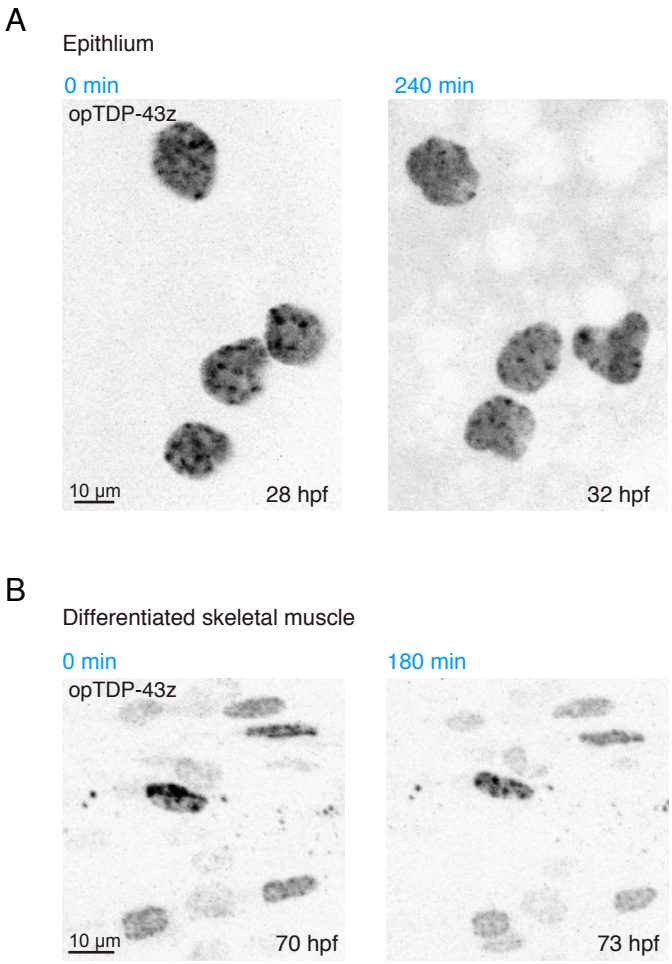

Asakawa et al. Figure S3